**Radiocommunication Study Groups**

## IAFI

## FURTHER UPDATES TO DRAFT WORKING DOCUMENT TOWARDS A PRELIMINARY DRAFT NEW REPORT ITU-R M.[IMT.ABOVE 100 GHz]

### 1.     Background

WP5D 40th meeting continued working on Report ITU-R M.[IMT.ABOVE 100 GHz] and it is expected that this work will continue in 41st meeting of WP5D. This Report is expected to compliment the Report ITU-R M.2376, which was completed in 2015 for studies of frequencies above 6 GHz for IMT technologies. During the development of Report ITU-R M.2376, studies from 10 GHz to 73 GHz were considered as per section 4.3 of that Report:

> **"4.3     Summary of the results of the studies**
>
> *In order to evaluate the feasibility of IMT in spectrum above 6 GHz, it is essential to understand how the radio signal will propagate in typical hotspot scenarios for IMT deployment. Both academia and industry have studied propagation characteristics of IMT deployment scenarios above 6 GHz, which are different from deployment scenarios for other services. Measurement campaigns that have been conducted cover frequency ranges from 10 GHz to 73 GHz. Both LoS and NLoS for indoor and outdoor, as well as outdoor-to-indoor measurement cases have been studied. Propagation pathloss has been investigated in order to estimate the coverage and link budget of the radio system. Other channel modelling and measurement activities have studied propagation phenomena, such as delay spread caused by multi-path propagation of radio signals, which can be helpful for system design. The results described in this Section support the feasibility of IMT in spectrum above 6GHz, and studies are continuing."*

It is envisioned that future IMT systems, in addition to other features, will need to support very high throughput data links to cope with the growth of the data traffic, new extremely bandwidth demanding use cases, as well as new capabilities of integrated sensing and communication.

Research and development is ongoing around the world to understand the suitability of mobile broadband systems in further higher frequency bands.

## 2. Discussions

While the earlier studies towards IMT identification in mm wave bands considered propagation studies and measurements up to 73 GHz, the current working document has been proposed for bands above 100 GHz. Current Radio Regulations already includes an allocation of a useful 13 GHz of spectrum to the Mobile service on primary basis in bands between 80-100 GHz is shown below:

**81-100 GHz**

| Allocation to services | | |
|---|---|---|
| **Region 1** | **Region 2** | **Region 3** |
| **81-84** | FIXED  5.338A<br>FIXED-SATELLITE (Earth-to-space)<br>MOBILE<br>MOBILE-SATELLITE (Earth-to-space)<br>RADIO ASTRONOMY<br>Space research (space-to-Earth)<br>5.149  5.561A | |
| **84-86** | FIXED  5.338A<br>FIXED-SATELLITE (Earth-to-space)  5.561B<br>MOBILE<br>RADIO ASTRONOMY<br>5.149 | |
| **86-92** | EARTH EXPLORATION-SATELLITE (passive)<br>RADIO ASTRONOMY<br>SPACE RESEARCH (passive)<br>5.340 | |
| **92-94** | FIXED  5.338A<br>MOBILE<br>RADIO ASTRONOMY<br>RADIOLOCATION<br>5.149 | |
| **94-94.1**  EARTH EXPLORATION-SATELLITE (active)<br>RADIOLOCATION<br>SPACE RESEARCH (active)<br>Radio astronomy<br>5.562  5.562A | | |
| **94.1-95**  FIXED<br>MOBILE<br>RADIO ASTRONOMY<br>RADIOLOCATION<br>5.149 | | |
| **95-100** | FIXED<br>MOBILE<br>RADIO ASTRONOMY<br>RADIOLOCATION<br>RADIONAVIGATION<br>RADIONAVIGATION-SATELLITE<br>5.149  5.554 | |

It is therefore considered desirable to study bands above 80 GHz in the current study.


**3.** **Proposal**

It is proposed that this new study should be cover bands above 80 GHz. Accordingly the draft working document has been suitably updated

**Radiocommunication Study Groups**

DRAFT WORKING DOCUMENT TOWARDS A PRELIMINARY DRAFT NEW
REPORT ITU-R M.[IMT.ABOVE ~~100 GHz~~80 GHZ]

*Editor's note: This working document includes text from all contributions submitted to ITU-R WP 5D #39. Square brackets around numbers (e.g. [XXX]) indicate the referenced input document to WP 5D #38. This document contains proposed text from [840], [841], [860], [863] and [877]. This document further contains proposed text from [929], [933], [975], [1026], [1046], [1053], [1054], and [1062] submitted to ITU-R WP 5D #40. In some cases, there is common proposed text for the outline [840,863] with both document numbers.*

**Technical feasibility of IMT in bands above ~~100 GHz~~80 GHz**

TABLE OF CONTENTS

*[Editor's note: ToC will be added later.]*

**1        Introduction**

[840,863] *[Editor's note: This section addresses background information of the study, including related activities, motivation etc.]*

[877] Report ITU-R M.2376 completed in 2015 was essential for pioneering studies of new frequency ranges (above 6 ~~100~~ GHz) for IMT technologies. Towards the future, it is envisioned that future IMT systems, in addition to other features, will need to support very high throughput data links to cope with the growth of the data traffic, new extremely bandwidth demanding use cases, as well as new capabilities of integrated sensing and communication (ISAC). There has been academic and industry

research and development ongoing related to suitability of mobile broadband systems in frequency bands above ~~100 GHz~~80 GHz to enable services requiring tera-bit per second speeds.

[1062] [This have prompted researchers to consider the technical feasibility of higher frequency bands in IMT. Although very high bands such as those above ~~100 GHz~~80 GHz have wide bandwidths, incumbent users and services need to be considered. However, this still means that a large number of frequency bands and continuous bandwidth have the opportunity to be allocated to IMT services.  It can be seen from the spectrum allocation of RR that a total of ~~97.21~~10.1 GHz in ~~100~~80-275 GHz is identified for mobile services, and a total of 137 GHz in 275-450 GHz can be used for LMS services. Although these frequency bands are also allocated to other types of services, there are problems of coexistence and interference, especially some passive services need to be protected.]

## 2      Scope

[840,863] This Report is to study and provide information on technical feasibility of IMT in bands above ~~100 GHz~~80 GHz and to complement the studies carried in Report ITU-R M.2376. This technical feasibility Report includes information on propagation mechanisms and channel models, as well as newly developed technology enablers such as active and passive components, antenna techniques, deployment architectures, and the results of simulations and performance tests.

**Commented [MC1]:** The precise frequency is open for further discussion.

## 3      Related documents

[863] Recommendation ITU-R M.[IMT.VISION 2030 AND BEYOND]

Report ITU-R M.[IMT.FUTURE TECHNOLOGY TRENDS]

Recommendation ITU-R P.525

Recommendation ITU-R P.676

Recommendation ITU-R P.838

Report ITU-R M.2376

Resolution ITU-R 56

Resolution ITU-R 65

Question ITU-R 229/5

Question ITU-R 262/5

*[Editor's note: To be added]*

## 4      Radio wave propagation in bands above ~~100 GHz~~80 GHz

[840] *[Editor's note: This section is expected to describe propagation mechanisms and channel models taking into consideration recently developed ITU-R Recommendations and Reports as well as new preliminary material contributed through research work done outside ITU-R to address propagation in frequencies above ~~100 GHz~~80 GHz.]*

[863] *[Editor's note: This section addresses the propagation information for radiowave in bands above ~~100 GHz~~80 GHz, including pathloss model, and other propagation characteristics. In addition, a comparison of channel characteristics above ~~100 GHz~~80 GHz and below ~~100 GHz~~80 GHz should also be given.]*

[841] [*Editor's note: 5D/841 proposed to leverage the detailed structure from Report ITU-R M.2376 for both the sub-clause 4 radio wave propagation and subclause 5 band characteristics*]

## 4.1 Propagation losses

[975] This section contains material which is the combination of existing ITU-R Recommendations and Reports as well as new preliminary material contributed through research work done outside ITU-R to address certain new use cases and applications. Further investigations are ongoing and applicable ITU-R Recommendations are being developed.

### 4.1.1 Basic transmission loss [Path loss]

*[Editor Notes: 4.1.1 Consolidated text, source: 933, 975]*

Understanding the propagation conditions are critical to designing an appropriate air interface and determining the type of hardware (particularly the array size) needed for reliable communications. Path loss, namely basic transmission loss, is the power attenuation caused by spreading of the electromagnetic energyas as well as characteristics of the environment. It governs the coverage distance and interference levels of a cellular system. An important characteristic of propagation above ~~100 GHz~~80 GHz is the significantly higher basic transmission loss   relative to traditional cellular bands. This high basic transmission loss is embodied in higher free space basic transmission loss and more significant atmospheric loss. Free-space basic transmission loss (dB) is given by equation 1,

$$L_p = 92.4 + 20 \log f + 20 \log d \tag{1}$$

where *f* is the frequency (GHz) and *d* is the distance (km) between transmitter and receiver (Recommendation ITU-R P.525-4). For example, an additional 36.9 dB and 40.8 dB of losses are expected to result in the ranges from 2 GHz to 140 GHz and 220 GHz respectively which will need to be compensated by some means, for example, larger antenna array sizes with higher antenna gains and MIMO technologies.

### 4.1.2 Atmospheric loss

*[Editor Notes: 4.1.2 Consolidated text, source: 975, 1062]*

Compared with mmWave, the atmospheric losses above ~~100 GHz~~80 GHz is mainly caused by gaseous absorption. The gaseous absorption by oxygen and water vapour (Recommendation ITU-R P.676) above ~~100 GHz~~80 GHz could be significant.  While oxygen absorption is dominant in some frequencies below ~~100 GHz~~80 GHz, such as the absorption peak near 60GHz, the water vapour absorption is dominant above 100GHz.  In addition, the effect of rain attenuation cannot be ignored. Fog, rain, snow, and dust losses are usually minor but may be important in some cases. Therefore, rain attenuation (Recommendation ITU-R P.838), fog attenuation (Recommendation ITU-R P.840), snow and dust attenuation need to be considered respectively, as needed.

The attenuation caused by atmospheric gases at 1-1000GHz is shown in Figure 1 taken from Recommendation ITU-R P.676. It shows the gaseous specific attenuation $\gamma_g$ (dB/km) as a function

of frequency[1]. The water vapour density is 7.5 g/m$^3$, the temperature is 15 °C and the pressure is 1 013.25 hPa (Standard) and a dry atmosphere (Dry).

As it is evident from Figure 1, the spectrum above ~~100 GHz~~80 GHz is punctuated by regions of very high absorption loss which will need to be factored in  any link budget in addition to the frequency-dependent path loss. This poses significant challenges in design and deployment of future IMT systems especially towards the top end of the spectrum above ~~100 GHz~~80 GHz.
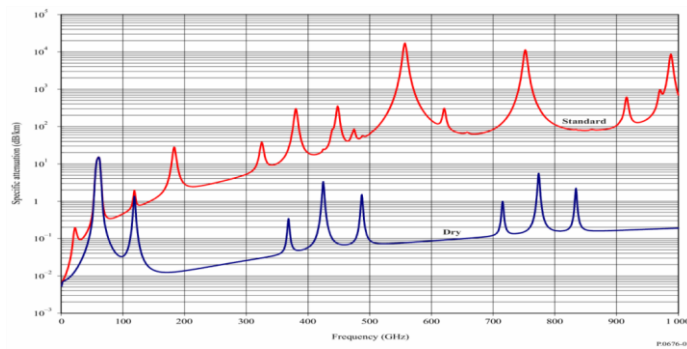
FIGURE 1

**Attenuation caused by atmospheric gases**



FIGURE 2

**Atmospheric gas attenuation, free space path loss, atmospheric gas attenuation and free space path loss attenuation (dB/Km)**
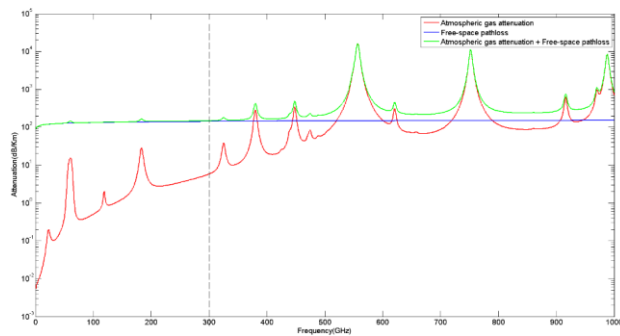


Figure 2 compares the attenuation results of atmospheric gas attenuation, free space path loss, atmospheric gas attenuation and free space path loss at a distance of 1000m. It can be found that when the frequency is less than 300 GHz, the free space path loss occupies a dominant position, and

_____

[1]  Assumptions used in Figure 1: [The water vapour density is 7.5 g/m$^3$, the temperature is 15 °C and the pressure is 1 013.25 hPa (Standard) and a dry atmosphere (Dry).]

the atmospheric gas attenuation is relatively small. When the frequency is greater than 300 GHz, the atmospheric gas attenuation rises rapidly with the increase of frequency and cannot be ignored.

For the 100-300 GHz frequency band, when the transmission distance is 200 m and 1000 m, the corresponding atmospheric gas attenuation is 0.106-1.293 dB and 0.53-5.72 dB; for the 300-450 GHz frequency band, when the transmission distance is 200 m and 1000 m, the corresponding Atmospheric gas attenuation is 1.29-68.76 and 6.45-343.8 dB.

Report ITU-R M.2376 provides that the atmospheric gas loss values of 28 GHz, 38 GHz, and 70-90 GHz respectively as 0.10 dB/Km, 0.15 dB/Km, 0.40 dB/km. It believes that gas attenuation could be of little concern when using these frequency bands to design urban microcellular mobile communications or backhaul for inter-site distances within 200 m. But for above ~~100 GHz~~80 GHz, in the same deployment situation, it is necessary to consider the atmospheric gas attenuation value as the link margin.

**Commented [RA2]:** I am not sure of the message in this part. It has a reasonable argument for short paths (system design) but it is not relevant for long paths (interference links). For long paths, e.g. from terrestrial to EESS space stations the attenuation could be significant even in frequencies below 300 GHz specially in absorption peaks neat 120 GHz and 180 GHz. It seems this is what the last paragraph wants to say but it is not clear. So, I think either this section needs to be rewritten or removed as it could be misleading.

### 4.1.3    Blocking loss and other losses

[975] The electromagnetic wave above ~~100 GHz~~80 GHz is sensitive to blocking. When an object blocks the propagation of the electromagnetic wave, it may cause penetration, reflection, scattering, and diffraction of electromagnetic wave. The penetration ability of electromagnetic wave above ~~100 GHz~~80 GHz is much weaker than that of low frequency. The penetration loss varies greatly with material properties. The measured penetration loss of clear glass can reach 27.6 dB/cm at 144 GHz while 4.4 dB/cm at 28 GHz [3]. The surface of common indoor building materials above ~~100 GHz~~80 GHz can no longer be regarded as smooth, and the reflection loss is very high. With the increase of frequency, the scattering power increases compared with the reflection power. The diffuse scattering is very weak in comparison to the specular reflection direction, but it is still theoretically high enough to enable the NLOS links on short distances [4]. Diffraction can usually be ignored, except the region close to the incident shadow boundary [5].

### 4.2    Recent activities on radiocommunication channel characteristics and modelling

[1062] Path Loss

To fulfil requirements of evaluate the coverage capability of IMT in bands above ~~100 GHz~~80 GHz, some research activities have been conducted recently to investigate the path loss of frequency bands ranged from 140 GHz to 330 GHz in Annex 2 and Annex 3. The propagation in indoor hotspot and short-distance scenarios have been studied. For indoor hotspot, the path loss is close to the free space path loss under Line-of-sight propagation condition. In some case like hallway, waveguide propagation effect can be observed. For short-distance, frequency dependence is close to free space propagation. And path loss variation over the measured bands is observed, which may be caused by atmosphere absorption.

•        Rain attenuation

Besides the clear advantages coming from the use of higher carrier frequencies, e.g. very large bandwidth and more compact equipment, high frequency electromagnetic waves are subject to impact induced by suspended water droplets (e.g. fog), gases (oxygen and water vapour) and hydrometers (e.g. rain, snow). Among them, rain plays the most relevant role. It absorbs and scatters electromagnetic energy, thus inducing impact on path loss of high frequency wireless signal.

In Annex 4, the dependence of rain attenuation on the rain drop dimension is investigated, i.e. so-called Drop Size Distribution (DSD). It is shown that compared with formulations in Recommendation ITU-R P.838-3 for the specific attenuation due to rain, the method taking into account the different impact of small and large drops, i.e. DSD data, can provide much better estimate of the rain attenuation.

## 4.3	Summary of the results of the studies

*[Editor's note: Review of this document at WP 5D #40 ended at section 4]*

## 5	Characteristics of IMT in bands above ~~100 GHz~~80 GHz

*[840,863] [Editor's note: This section is expected to describe the characteristics of IMT in frequencies above ~~100 GHz~~80 GHz, including coverage, link budget, applicable bandwidth and needed capabilities to support new usages and deployment scenarios, etc]*

*[863] [Editor's note: This section addresses the analysis of IMT technologies deployment in bands above ~~100 GHz~~80 GHz, including coverage, link budget, mobility, the impact of ultra-large bandwidth and needed capabilities to support new deployment scenarios etc.]*

*[841] [Editor's note: 5D/841 proposed to leverage the detailed structure from Report ITU-R M.2376 for both the subclause 4 radio wave propagation and subclause 5 band characteristics. 1*

### 5.1	Outdoor-to-outdoor coverage and link budget

[1053] Main penalties for coverage are the increased free space path loss at higher frequencies and reduced available output power of PAs, further reduced by required back off due to the PAPR of the signal. The Figure 1 below (taken from [1]) shows this dependency.

FIGURE 1

**Achievable distance versus frequency for fixed EIRP (100 Gbps, LoS)**
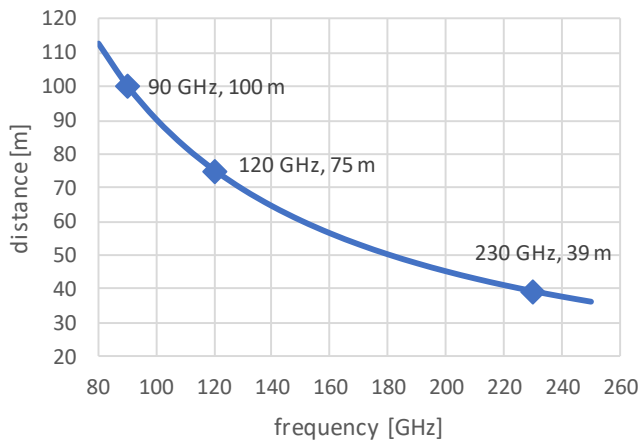


To assess the feasibility and identify the tx power requirements for a certain coverage, among the use cases discussed for 6G bands above ~~100 GHz~~80 GHz the high data rate hot spot scenario has been considered in [1]. Main assumptions were a range of up to 100 m and a target data rate of 100 Gbit/s in a 10 GHz bandwidth and using cross-polarization and two parallel streams per polarization (i.e., 4x4 LoS-MIMO). Since wall penetration and reflection above ~~100 GHz~~80 GHz is not well assessed, but known to be challenging, the analysis has been done for Line-of-Sight (LOS).

A simplified link budget given in [1] for a carrier frequency of 120 GHz shows a required total e.i.r.p. of about 63 dBm to achieve the 100 Gbit/s with 100 m range.

TABLE 1

**Link budget examples [1][1]**

| carrier frequency [GHz] | 120 | 120 | GHz |
|---|---|---|---|
| 2 polarizations | 4 | 4 | parallel streams |
| bandwidth | 10 | 10 | GHz |
| **target rate** | **100** | **10** | **Gbit/s** |
| spectral efficiency | 2,50 | 0,25 | bit/s/Hz |
| required SNR [lin] | 4,66 | 0,19 | |
| required SNR [dB] | 6,68 | -7,23 | dB |
| Noise power [dBm] | -74 | -74 | dBm |
| Noise figure [dB] | 10 | 10 | dB |
| Rx signal power [dBm] | -57,32 | -71,23 | dBm |
| Distance [m] | 100 | 100 | m |
| Free space path loss [dB] | 114,03 | 114,03 | dB |
| tx EIRP [dBm] per stream | 56,71 | 42,79 | dBm |
| **total tx EIRP [dBm]** | **62,73** | **48,82** | **dBm** |

The total tx output power can be achieved by using high gain antennas and individual Pas per antenna element. The impact of increasing frequency from 90 GHz to 230 GHz is considered in the following range analysis example taken from [1], which shows the major dependencies of array size and achievable range for the assumption that the achievable tx power per antenna element will be reduced by physical limitations of technology as further detailed e.g. in [2].

TABLE 2

**Link budget examples for increasing frequency [1]**

| carrier frequency [GHz] | 90 | 120 | 230 | 120 | 230 | GHz |
|---|---|---|---|---|---|---|
| no. of parallel streams | 2 | 2 | 2 | 2 | 2 | |
| bandwidth [GHz] | 10 | 10 | 10 | 10 | 10 | GHz |
| target rate [Gbit/s] | 100 | 100 | 100 | 100 | 100 | Gb/s |
| spectral efficiency per stream [bit/s/Hz] | 5 | 5 | 5 | 5 | 5 | b/s/Hz |
| **tx output power [dBm]** | **18** | **15** | **12** | **15** | **12** | **dBm** |
| array element gain [dB] | 5 | 5 | 5 | 5 | 5 | dBm |
| **number of array elements** | **64** | **64** | **64** | **120** | **320** | |
| array + power gain [dB] | 36,12 | 36,12 | 36,12 | 41,58 | 50,10 | dB |
| total tx EIRP [dBm] | 59,12 | 56,12 | 53,12 | 61,58 | 67,10 | dBm |
| **tx EIRP per stream [dBm]** | **56,12** | **53,12** | **50,12** | **58,58** | **64,10** | **dBm** |
| required SNR [lin] (Shannon) | 31 | 31 | 31 | 31 | 31 | |
| Shannon required SNR [dB] (Shannon) | 14,91 | 14,91 | 14,91 | 14,91 | 14,91 | dB |
| Noise power [dBm] in bandwidth | -74 | -74 | -74 | -74 | -74 | dBm |
| Noise figure [dB] | 10 | 10 | 10 | 10 | 10 | dB |
| min. Rx signal power [dBm] per stream | -49,09 | -49,09 | -49,09 | -49,09 | -49,09 | dBm |
| allowed path loss (LOS) | 105,21 | 102,21 | 99,21 | 107,67 | 113,19 | dB |
| **Distance [m]** | **48,32** | **25,66** | **9,48** | **48,11** | **47,39** | **m** |

Table 2 shows link budgets taken from [1] for the case of 48 m range and 2 parallel streams with a total data rate of 100 Gbit/s. This takes into account the effects of reduced available PA output power with increasing frequency and compensating that with increased number of transmit chains and resulting in increased array gain. Major outcome was that the 48 m range with 100 Gbit/s can be achieved with PA per array element of 12-15 dBm if the number of PAs and array elements is increased from 64 to 120 at 120 GHz and up to 320 at 230 GHz. Such devices are existing as presented in [3], [4].The required number of array elements depends on carrier frequency and back-off and might be further increased from 120 (120 GHz, back-off 0 dBdb) up to 716 (230 GHz, back-off 7 dB) [1]. In this way achievable range can be increased with a combination of total transmit power increase and antenna aperture increase.

The required phased array technology to realize the needed architecture is basically available and will further be enhanced. In [3] an 8 x 16 array for D-band is described, with tx output power ($P_{1dB}$) of 10 dBm. With such devices the technology is close to the requirements given by the examples described above. Also, full integration of multiple array tiles to realize large arrays with more than 300 elements has been described in [4].

Impact of PAPR:

PAPR of the transmitted signal requires power back-off , which reduces the achievable total tx output power. Reducing PAPR can increase tx output power of a given device and therefore either increase range or limit the number of array elements and array gain. Used waveforms have a crucial role here. Whereas scaling up of OFDM signal formats used in lower bands also maintains the high PAPR, other waveforms like single-carrier with frequency domain equalization (SC-FDE) show less PAPR at comparable processing complexity. Also, impact of hardware limitations is lower. In [5] different waveforms have been compared with respect to PAPR and sensitivity to hardware impairments. An improvement of 5.5 dB in PAPR compared to OFDM can be achieved. Further improvement with specific ring constellation signal formats show that additional gain of 1.5 dB is feasible. Significantly reduced phase noise sensitivity with low complexity phase noise compensation algorithm was shown.

So, with using an appropriate waveform with reduced PAPR the system requirements for a certain coverage in terms of tx capabilities, array gain and array size can be either relaxed, or with the same settings the coverage can further be increased due to the now available higher average tx power.

**5.2      Outdoor-to-indoor coverage**

**5.3      Mobility**

**5.4      Impact of bandwidth**

**5.5      Channel Sparsity**

[975] A sparse representation is one in which a small number of coefficients contain a large proportion of the energy [6]. For a multi-antenna system, the channel sparsity can be expressed in both the angular domain and delay domain and the low rank of the channel matrix. It is often claimed that millimeter wave (usually, 30-300 GHz) channels are 'sparse', i.e., have few entries in the delay angle bins (Report ITU-R M.2412). The channel above ~~100 GHz~~80 GHz is more likely to be sparse due to the weak diffraction ability [7][8].6 Enabling technologies toward IMT in bands above ~~100 GHz~~80 GHz

[840, 863] *[Editor's note: This section [840] [is expected to describe] [863] [addresses] newly developed technology enablers including active and passive components, antenna techniques, advancement in material sciences, etc.]*

[840]

[1053] Based on the analysis in [6] [10] and [7] [11], there are some technical aspects need to be study and investigated  so that  mobile communications in the  very high frequency range can be enabled  To overcome changing related to power consumption of both base stations and mobile devices the need to be study and analysed, e.g.  directions:

1. Study key RF frontend and digital baseband implementations that focuses on energy efficiency. A first step is to investigate energy efficient RF transceiver front-ends. Once this is accomplished, a second step is to adapt accordingly digital baseband implementations as well as higher layers of the communication systems.

2. The beam management needs to be adapted to the corresponding antenna arrays at both base stations as well as mobile devices. Especially for mobile devices, it needs to be ensured that effective and efficient reception and transmission is possible in all directions that are expected to be used for communication.

3. Integration with sensing, communication at lower carrier frequencies and other side information. Due to propagation conditions and other implementation challenges one of the key aspects will be the tight integration with other systems providing information to assist assists communications at carrier frequencies in the very high range Above 100 GHz80 GHz.

## 6 Enabling technologies toward IMT in frequencies above 100 GHz80 GHz

*[Editor's note: This section is expected to describe newly developed technology enablers including active and passive components, antenna techniques, advancement in material sciences, etc.]*

*{Note from the BR: This title and note has been added post WP5D #40 (source 5D/840). It's also to be noted, that sections 6.1.1.-6.1.6 are existing twice in this document.}*

### 6.1 Antenna technology

*[Editor's note: during the discussion the term antenna technologies was suggested to be rephrased, to reflect advances in Antenna design]*

[1053] Antenna element (AE) pitch in an antenna array system (AAS) is roughly 1.5 mm ($\lambda$/2) at 100 GHz80 GHz. Assuming that each RFIC supports 16 AEs, the area available for a transceiver integrated circuit (IC) (consisting of both Rx and Tx circuits) is typically less than 6 mm x 6 mm. For higher frequencies, or when supporting less AEs per IC, the area becomes even smaller, as shown by Table 3. Therefore, high level of integration must be on top priority to consider when it comes to hardware implementation. In view of the large number of AEs and the limited space available for each RFIC, the only feasible technology of integration and interconnect is the antenna-in-package (AiP) approach in which the active chips are embedded in the package and the routing is made in the fan-out distribution layer, with AEs being fabricated on top of the package, as Figure 2 shows. The solution is foreseen to be applicable up to 200 GHz at least. Development of the AiP technology for above 100 GHz80 GHz has been active both in industry and academia in recent years. The national project in Germany, 6GKom, is a typical example where D-band (110-170 GHz) AAS is being developed and the results achieved so far are very promising.
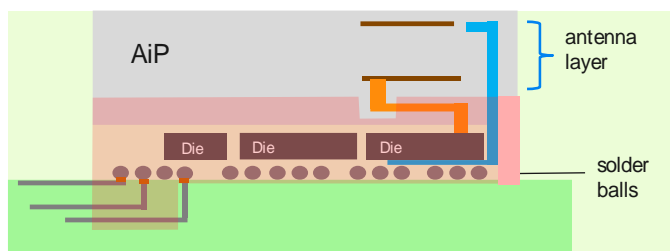
TABLE 3

**Available area per RFIC in an antenna array for frequencies above ~~100 GHz~~80 GHz**

| Frequency (GHz) | 100 | 150 | 200 | 250 | 300 |
|---|---|---|---|---|---|
| AE pitch ($\lambda/2$) (mm) | 1.5 | 1.0 | 0.75 | 0.6 | 0.5 |
| RFIC area with 4 AEs (mm x mm) | 3.0 x 3.0 | 2.0 x 2.0 | 1.5 x 1.5 | 1.2 x 1.2 | 1.0 x 1.0 |
| RFIC area with 16 AEs (mm x mm) | 6.0 x 6.0 | 4.0 x 4.0 | 3.0 x 3.0 | 2.4 x 2.4 | 2.0 x 2.0 |

FIGURE 2

**A conceptual drawing of basic AiP build up (the thick orange line is the RF routing path)**



### Directional antennas and pencil beamforming

[*1046*] The limited transmission power of transceivers in frequencies above ~~100 GHz~~80 GHz, combined with the high propagation losses at these frequencies (resulting mostly from the small effective area of antennas, when operating within the molecular absorption free bands of the spectrum above ~~100 GHz~~80 GHz), require the utilization of high-gain directional antennas and pencil beamforming techniques at the transmitter and the receiver of a communication link. Usually, in the literature, such antennas are assumed to be static, and the problem is mostly in determining the correct direction and the optimal antenna (array) pattern in order to maximize the antenna/beamforming gain. However, sustaining perfectly aligned transmitter and receiver antennas and /or optimal antenna (array) patterns in practical scenarios is not always feasible, due to various factors, such as thermal expansion, dynamic wind loads, weak earthquakes and other physical phenomena causing vibrations of the transceivers antennas. These phenomena result in -often severe- beam misalignment. Moreover, estimation errors in the angle of arrival or angle of departure as well as hardware imperfections in the antenna array, which include array perturbation and mutual coupling, and, most importantly, mobility in various random trajectories, may cause stochastic tracking estimation errors. Robust beamforming and tracking techniques, capable of supporting adaptation to the particularities of challenging usage scenarios, are therefore key performance factors.

In addition to high propagation losses, THz signals can be obstructed (i.e., absorbed, reflected or diffracted) by different types of obstacles (e.g. people, furniture, walls, windows etc). These obstructing obstacles can create a shadow area which might (partially) block the receiver antenna effective area. Moreover, the obstacle itself might reflect and/or absorb the signal. As much as directionality and pencil beamforming are necessary to ensure connectivity reliability in the above ~~100 GHz~~80 GHz regime, they may, at the same time, intensify the blockage challenges. Incorporating Reconfigurable Intelligent Surfaces (RIS) is a way to overcome blockage and reduce blocking probability.

### 6.1.1 Photo-Conductive lens antenna

[1062] Illuminated under laser beams of certain frequencies, some semiconductor substrates (e.g. InP and GaAs) can generate photoconduction current. The photocurrent can then radiate as THz wave in space by biased antenna electrodes. In this way, Photo-conductive antenna can convert photonic energy to THz radiation.

Such photo conversion usually has a low conversion efficiency, resulting in low radiated power of the antenna (uW). Therefore, the integration of dielectric lens can be used to focalize the radiated beams and eventually increase antenna gain.

### 6.1.2 Reflect-array and Transmit-array

[1062] Reflect-array consists of electromagnetic scatters printed on a surface. With carefully designing the phase shift of each scatter, the Reflect-array can reflect a predetermined beam, behaving similar as curved reflector surface.

Similarly, Transmit-array consists of a planar substrate with a number of printed resonators with designed phase distribution. The incident wave from focal source is then converted into the desires beam pattern when passing through the transmit-array plane.

Reflect-array and Transmit-array are applicable to many applications, e.g. range extension and high-gain antennas. With the merits of low profile, high efficiency and reconfigurable, they are promising candidates for next-generation communication.

FIGURE 6.X

**Reflect-array and Transmit-array**
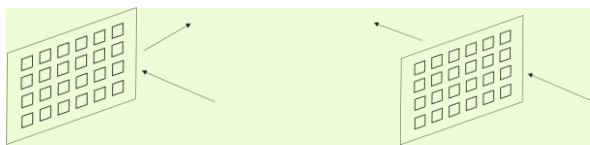


### 6.1.3 Metasurfaces

[1062] Metrasurfaces are artificial structure that are engineered to obtain unusual properties, such as negative refraction, perfect lensing or superlensing. In Metrasurfaces, each unit cell element can be controlled independently with tunable element, thus having a frequency response of specific amplitude and phase values. Together, Metrasurfaces form an electromagnetically interconnected network towards a specific functionality e.g. wave absorption, surface wave cancellation, antenna decoupling and beam shaping.

Metasurfaces have the potential to enable attractive radiating solutions, for example, a smart metasurface glass which can be programed to different statuses of full penetration, partial reflection, or full reflection for the incident radio waves, thus providing different communication performance according to required circumstances.

### 6.1.4 Nano-Photodetectors

[1062] With the developments of nanotechnology, nano-photodectectors have the potential to be a portable, cost effective and power efficient solution for "above 1 THz" imaging system. On example is carbon nanotube (CNT) sensing array which can convert the illuminating THz radiation to a measurable photocurrent according to the photothermoelectric effect.

Similarly, the graphene photodetector can also transform the illuminating THz radiation to a measurable photocurrent in a similar way to CNT. Graphene's transparency makes its applicability to being integrated into screen antenna, intelligent glasses, etc.

### 6.1.5 Antenna-on-Chip and Antenna-in-Package

[1062] Antenna-on-Chip is a possible way for THz application which directly integrates the antenna with the front-end circuit on a silicon substrate. Antenna-on-Chip has advantages of high level of integration, lower interconnect loss and robustness due to no external bonding wires. At the same time, on-chip antenna design is also challenging. For example, the surface waves generated in substrates will interfere with the antenna radiation and degrade the performance. Sophisticate solutions are needed to overcome these barriers.

Antenna-in-package is another way to achieve the integration of antenna and the front-end circuit. Compared with the on-chip solution, the interconnect loss increases, especially for THz frequencies. Effective packaging techniques are needed to minimize the losses.

### 6.1.6 Orbital Angular Momentum

[1062] Besides the traditional way of multiplexing through space, frequency, time, code and polarization, Orbit Angular Momentum (OAM) provides a new dimension of multiplexing. In OAM, each antenna is associated with a different orbital momentum, thus generating orthogonal modes to carry different information. For example, combined OAM and massive MIMO can greatly boost the data rate and achieve higher spectrum sufficiency.

OAM is a promising candidate technology for future wireless communications. The main research challenges involves enabling mobility usage scenarios, including simple user-equipment side antennas to demodulate OAM signals.

*[Editor's Notes: 6.1 Consolidated text, source:1053 and 1062. Contribution [1046] needs to be moved to a separate section at the end of chapter 6, that is 6.4.]*

> **Commented [AA3]:** An edited version of these paragraphs is proposed highlighted in yellow. If this edited version is accepted, these paragraphs should be deleted.

The limited transmission power of transceivers in frequencies above ~~100 GHz~~80 GHz, combined with the high propagation losses at these frequencies (resulting mostly from the small effective area of antennas, when operating within the molecular absorption free bands of the spectrum above ~~100 GHz~~80 GHz), could require the utilization of high-gain directional antennas and pencil beamforming techniques at the transmitter and the receiver of a communication link. In addition to high basic transmission losses, propagation of radio waves above ~~100 GHz~~80 GHz can be impaired (i.e., absorbed, reflected, scattered or diffracted) by various types of obstacles (e.g. people, furniture, walls, windows etc). These obstacles can create a shadow area which might (partially) block the receiver antenna's effective aperture. Moreover, the obstacle itself might reflect and/or absorb the signal. Some enabling antenna technologies proposed as potential ways to overcome these challenges are presented in the following sections .

> **Commented [RA4]:** Diffraction, reflection, etc are all propagation mechanisms. What is meant here is in addition to basic transmission loss.

> **Commented [RA5]:** This is presented as a genera statement. While this is true for many applications it is not the case for all. Also, the point about the need for highly directional antenna is made at the beginning of the paragraph. So, this sentence is not needed.

> **Commented [Lin Hui6]:** This paragraph is from the input of WWRF 1046. As a new section 6.4 was added to include all text from 1046. We don't need this paragraph here, suggest to delete.

### 6.1.1 Photo-Conductive lens antenna

Illuminated under laser beams of certain frequencies, some semiconductor substrates (e.g. InP and GaAs) can generate photoconduction current. The photocurrent can then radiate as THz wave in space by biased antenna electrodes. In this way, photo-conductive antenna can convert photonic energy to THz radiation.

Such photo conversion usually has a low conversion efficiency, resulting in low radiated power of the antenna ($\mu$W). Therefore, the integration of dielectric lens can be used to focalize the radiated beams and eventually increase antenna gain.

### 6.1.2 Reflect-array and Transmit-array

Reflect-array consists of electromagnetic scatterers printed on a surface. With carefully designing the phase shift of each scatterer, the Reflect-array can reflect a predetermined beam, behaving similar as curved reflector surface.

Similarly, Transmit-array consists of a planar substrate with a number of printed resonators with designed phase distribution. The incident wave from focal source is then converted into the desired beam pattern when passing through the transmit-array plane.

Reflect-array and Transmit-array are applicable to many applications, e.g. range extension and high-gain antennas. With the merits of low profile, high efficiency and reconfigurability, they are promising candidates for next-generation communication.

FIGURE 6.X

**Reflect-array and Transmit-array**
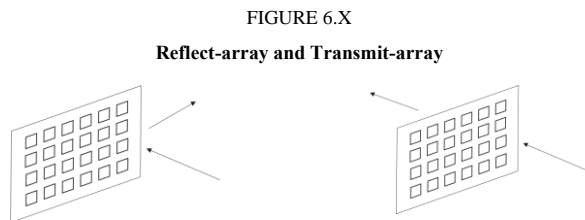


### 6.1.3 Metasurfaces

Metrasurfaces are artificial structures engineered to obtain unusual properties, such as negative refraction, perfect lensing or superlensing. In Metrasurfaces, each unit cell element can be tuned independently, thus having a frequency response of specific amplitude and phase values. Metrasurfaces form an electromagnetically interconnected network towards a specific functionality e.g. wave absorption, surface wave cancellation, antenna decoupling and beam shaping.

Metasurfaces have the potential to enable various radiating behaviours, for example, a smart metasurface glass which can be programmed to different statuses of full penetration, partial reflection, or full reflection for the incident radio waves, thus providing different communication performance according to required circumstances.

### 6.1.4 Nano-Photodetectors

With the developments of nanotechnology, nano-photodectectors have the potential to be a portable, cost effective and power efficient solution for "above 1 THz" imaging system. On example is carbon nanotube (CNT) sensing array which can convert the illuminating THz radiation to a measurable photocurrent according to the photothermoelectric effect.

Similarly, the graphene photodetector can also transform the illuminating THz radiation to a measurable photocurrent in a similar way to CNT. Graphene's transparency allows integration into screen antenna, intelligent glasses, etc.

### 6.1.5 Antenna-on-Chip and Antenna-in-Package

Antenna-on-Chip is a possible way for THz application which directly integrates the antenna with the front-end circuit on a silicon substrate. Antenna-on-Chip has advantages of high level of integration, lower interconnect loss and robustness due to no external bonding wires. At the same time, on-chip antenna design is also challenging. For example, the surface waves generated in

- 17 -

substrates will interfere with the antenna radiation and degrade the performance. Sophisticated solutions are needed to overcome these barriers.

Antenna-in-package is another way to achieve the integration of antenna and the front-end circuit. Compared with the on-chip solution, the interconnect loss increases, especially for THz frequencies. Effective packaging techniques are needed to minimize the losses.

Antenna element (AE) pitch in an antenna array system is roughly 1.5 mm (λ/2) at ~~100 GHz~~80 GHz. Assuming that each RFIC supports 16 AEs, the area available for a transceiver integrated circuit (IC) (consisting of both Rx and Tx circuits) is typically less than 6 mm x 6 mm. For higher frequencies, or when supporting less AEs per IC, the area becomes even smaller, as shown in Table 3. Therefore, high level of integration must be on top priority to consider when it comes to hardware implementation. In view of the large number of AEs and the limited space available for each RFIC, the only feasible technology of integration and interconnect is the antenna-in-package (AiP) approach in which the active chips are embedded in the package and the routing is made in the fan-out distribution layer, with AEs being fabricated on top of the package, as Figure 2 shows. The solution is foreseen to be applicable up to 200 GHz at least. Development of the AiP technology for above ~~100 GHz~~80 GHz has been active both in industry and academia in recent years. The national project in Germany, 6GKom, is a typical example where D-band (110-170 GHz) antenna arrays are being developed and the results achieved so far are very promising.
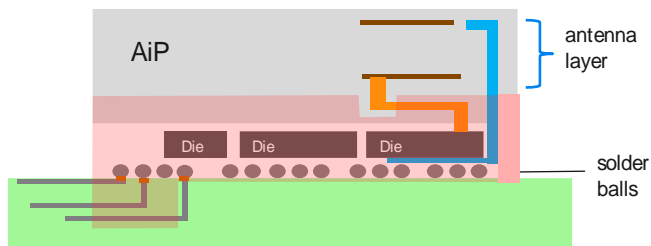
TABLE 3

**Available area per RFIC in an antenna array for frequencies above ~~100 GHz~~80 GHz**

| Frequency (GHz) | 100 | 150 | 200 | 250 | 300 |
|---|---|---|---|---|---|
| AE pitch (λ/2) (mm) | 1.5 | 1.0 | 0.75 | 0.6 | 0.5 |
| RFIC area with 4 AEs (mm x mm) | 3.0 x 3.0 | 2.0 x 2.0 | 1.5 x 1.5 | 1.2 x 1.2 | 1.0 x 1.0 |
| RFIC area with 16 AEs (mm x mm) | 6.0 x 6.0 | 4.0 x 4.0 | 3.0 x 3.0 | 2.4 x 2.4 | 2.0 x 2.0 |

FIGURE 2

**A conceptual drawing of basic AiP build up (the thick orange line is the RF routing path)**



### 6.1.6 Orbital Angular Momentum

Besides the traditional way of multiplexing through space, frequency, time, code and polarization, Orbit Angular Momentum (OAM) provides a new dimension of multiplexing. In OAM, each antenna is associated with a different orbital momentum, thus generating orthogonal modes to carry different information. For example, combined OAM and massive MIMO can greatly boost the data rate and achieve higher spectrum sufficiency.

OAM is a promising candidate technology for future wireless communications. The main research challenges involves enabling mobility usage scenarios, including simple user-equipment side antennas to demodulate OAM signals.

## 6.2 Semiconductor technology

[1053] The performance of THz circuits and systems is constrained by the performance of active devices (e.g., transistors) and passive elements. Fortunately, semiconductor technologies have progressed so much in the past 1-2 decades that multiple options are available nowadays in choice of device technology capable to support >~~100 GHz~~80 GHz applications. Figure 3 shows two featuring parameters that are used to characterize the speed of a transistor, fmax and fT. As seen from the figure, the fmax of InP and GaAs transistors have exceeded 1 THz. Even SiGe has reached speed towards 700 GHz fmax and has good potential to extend its region of operation further to 1 THz band in future. It should be noted that these are the speed of the intrinsic transistors. In reality, the usable speed of the transistors is very much reduced due to parasitic effects which degrade the circuits performance more and more when the operation frequency goes higher and higher. The reduction in fT/fmax can be as large as 30%. In order to obtain decent gain and efficiency, the operation frequency is usually chosen to be in the range of ¼ to ½ of the intrinsic fT/fmax, as a role of thumb. Even when this role is followed, it can be seen from Figure 3 that *active circuits can deliver decent performance at operation frequency of 100-300 GHz, without necessarily relying on harmonics to generate THz signals.*

FIGURE 3

**Overview of fmax and fT performance of state-of-the-art semiconductor technologies [8]**
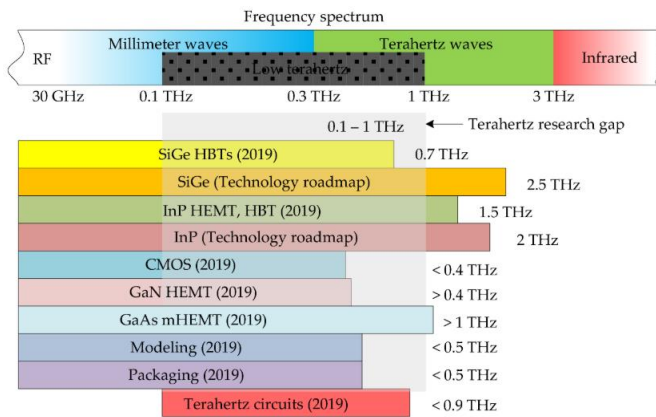


Commercial-friendly Gallium-Arsenide (**GaAs**) process, e.g., 100 nm pHEMT, supports operation up to the high W-band (~115 GHz). Its metamorphic version, mHEMT, is much faster. Combining with down-scaling to e.g., 20 nm, GaAs mHEMT devices have demonstrated fmax of 1.2 THz. Therefore, the technology can comfortably support circuits operating at 100-500 GHz range. The drawback with GaAs is its relatively low integration capability. Indium Phosphide (**InP**) is even faster and has better integration possibility than GaAs. With 25 nm node, 1.5 THz fmax and an associated 0.61 THz fT were demonstrated in 2015. A 10-stage amplifier fabricated in this process delivered 9 dB power gain at 1.03 THz. The downside with InP is its relatively high manufacturing cost and the lack of the possibility to integrate complex analog and digital multiple functions. The

**Commented [RA7]:** What is the applicability to above 100 GHz? As far as I know, OAM could also be implemented in lower bands. What is the significance of it for above 100 GHz? Maybe delete?

**Commented [AA8]:** This subsection does not belong in 6.1. We may want to introduce another chapter on MUX and include there OAM

**Commented [Lin Hui9]:** As contributor of this subsection 6.1.6, we agree with above comments, either delete or move is fine for us.

relatively newer GaN technology offers several advantages over GaAs and InP, however, the current GaN devices are not fast enough to be commercially used for frequencies well above ~~100 GHz~~80 GHz. Evolution of the GaN HEMT is happening and it can become a favorable technology for above ~~100 GHz~~80 GHz in the future.

As high integration capability is a profound requirement for above ~~100 GHz~~80 GHz AAS, neither GaAs nor InP semiconductor technology is seen as appropriate for 6G radio systems. In this context, the silicon-based technology, complementary metal oxide semiconductor (**CMOS**) and silicon germanium (**SiGe**), are considered to be the feasible technologies, owing to their cost and integration advantages over the III-V compounds technologies.  As a result of the European effort and investment, the most advanced SiGe HBTs with peak fT of 505GHz and peak fmax of 720 GHz were recently demonstrated on the research level. Industrialization of this technology, which results in a lower fmax of slightly below 600 GHz, is currently in its qualification phase and release for engineering is anticipated in 1-2 years. Even the commercially available SiGe process today, e.g., B11HFC from Infineon [9], has fmax and fT of 435 GHz and 250 GHz, respectively, which is proven to support circuits and systems operating up to 250 GHz, with 30 GHz bandwidth (~150 GHz). Figure 4 shows the evolution of the SiGe HBT technology over the last four decades in terms of fmax, fT and gate delay. The progress in recent years is obvious and impressive. It is believed that CMOS, especially SiGe, will play a dominant role in research and development of beyond 5G communication systems, particularly in the sub-THz band (100-300 GHz).

FIGURE 4

**Evolution of transistor figure of merits for SiGe HBTs**
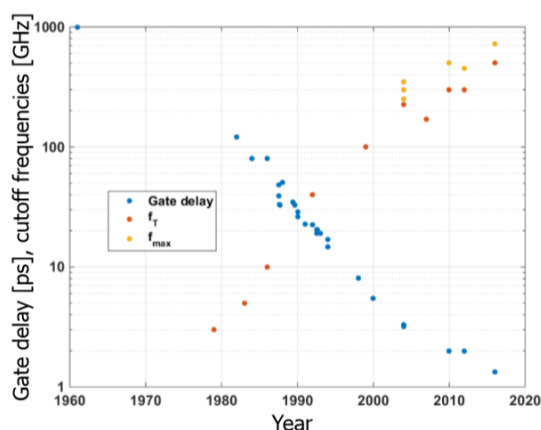


However, what should be aware of is that the silicon-based technologies are not capable to deliver similar performance as the III-V technologies do. Often and mostly, performance comparison of semiconductor technologies is given for the transmitter (Tx) side, focusing on power amplifiers (PAs). Here, technology comparison is done for (the relatively-less investigated) receivers operating in the whole millimeter-wave band (30-300 GHz), focusing on low-noise amplifiers (LNAs). Figure 5 compares the noise figure (NF) of LNA ICs in different technologies. Clearly, GaAs and InP offer much better NF than CMOS and SiGe. When the frequency approaches 300 GHz, the noise figure from the silicon-based technology is so high that the technology is only capable to support indoor use cases or outdoor communications with limited range.

FIGURE 5

**Noise figure data of LNA ICs in CMOS (green circle), SiGe (orange circle), GaAs (red triangle) and InP (black square). The lines are exponentially fitted to the best NF of the respective technologies**
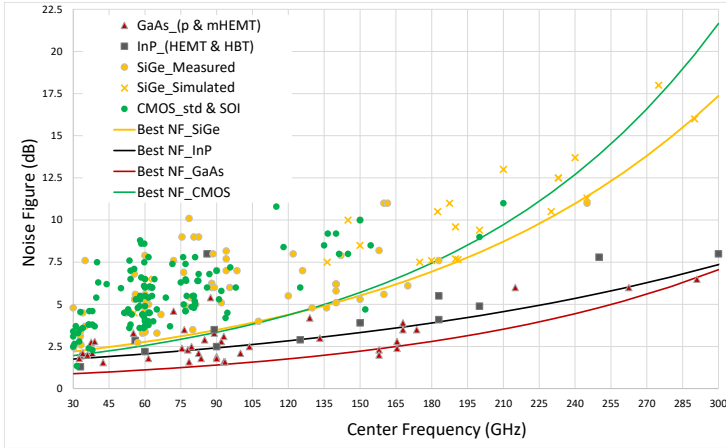


It is interesting to note that a simple exponential fit to the best NF (lowest value) applies to all technologies across the whole millimeter-wave range (30-300 GHz). The fitting parameters are given in Table 4, which can be used as an empirical model for best NF in the corresponding technology frequencies above ~~100 GHz~~80 GHz.

TABLE 4

**Empirical expressions of the best LNA noise figure achieved by different technologies based on published work ($f_c$ = operation frequency)**

| Technology | Empirical model |
|---|---|
| CMOS LNA | $\min NF = 1.50 \exp\left(\frac{f_c}{112.4}\right)$ |
| SiGe LNA | $\min NF = 1.75 \exp\left(\frac{f_c}{130.7}\right)$ |
| GaAs LNA | $\min NF = 0.70 \exp\left(\frac{f_c}{129.9}\right)$ |
| InP LNA | $\min NF = 1.50 \exp\left(\frac{f_c}{188.7}\right)$ |

The above NF analysis reveals that CMOS and SiGe are the optimal candidates offering a balanced in terms of integration and Rx noise figure for the 170 GHz band and below. For frequencies above 170 GHz, there is no single technology that meet both requirements, thus, smart and advanced heterogeneous combination of the technologies can become necessary.

## 6.3 Material technology

**Reconfigurable Intelligent Surfaces (RIS)**

[1046] One of the major challenges of operating in above ~~100 GHz~~80 GHz band is the obstructed propagation environment due to high propagation loss and blockage. RISs have been explored as a

potential solution towards sustaining non line-of-sight communication, introduce reconfigurability and programmability of the wireless propagation channel and ensuring communication at higher frequency with mobile objects. RISs comprise of multiple elements ('unit cells') and, by tuning their phase shifts, it is possible to control the propagation direction of impinging electromagnetic waves. RISs can reflect the waves in a particular direction and can impact the phase of the reflected wave. RISs have been explored for both indoor and outdoor network environments and the initial prototypes have demonstrated their potential in aiding communication at high frequency bands. RISs are also considered as a key enabler for Terahertz communications, though there are multiple challenges that need to be addressed before RISs are adopted. Ensuring smooth RIS operation supporting reconfigurability, where mobile users are involved, requires a control system architecture that empowers tunable / programmable RIS operation, e.g. with respect to the desired beam steering and beamforming. Moreover, the controller design needs to take the contextual information into consideration, to reduce the vulnerability due to blockages and sustain the communication for mobile users. Gathering the contextual information can lead to high computational overhead and delays in the controller mechanism. Another challenge is the channel estimation as multiple channels might be involved. In a nutshell, RISs are considered as a promising technology for above ~~100 GHz~~80 GHz network operation but also pose several design and optimization challenges.

## 6.4 MIMO and Beamforming

### 6.4.1 Directional antennas and pencil beamforming

[1046] The limited transmission power of transceivers in the above ~~100 GHz~~80 GHz frequency regime, combined with the high propagation losses at these frequencies require the utilization of high-gain transmit and receive antennas, either by employing directions antenna technologies or pencil beamforming techniques, utilizing multi-element antenna arrays. Usually, in the literature, such antennas are assumed to be static, and the problem is mostly in determining the correct direction and the optimal antenna (array) pattern in order to maximize the antenna/beamforming gain. However, sustaining perfectly aligned transmitter and receiver antennas and /or optimal antenna (array) patterns in practical scenarios is not always feasible, due to various factors, such as thermal expansion, dynamic wind loads, weak earthquakes and other physical phenomena causing vibrations of the transceivers antennas. These phenomena result in -often severe- beam misalignment. Moreover, estimation errors in the angle of arrival or angle of departure as well as hardware imperfections in the antenna array, which include array perturbation and mutual coupling, and, most importantly, mobility in various random trajectories, may cause stochastic tracking estimation errors. Robust beamforming and tracking techniques, capable of supporting adaptation to the particularities of challenging usage scenarios, are therefore key performance factors.

In addition to high propagation losses, THz signals can be obstructed (i.e., absorbed, reflected or diffracted) by different types of obstacles (e.g. people, furniture, walls, windows etc). These obstructing obstacles can create a shadow area which might (partially) block the receiver antenna effective area. Moreover, the obstacle itself might reflect and/or absorb the signal. As much as directionality and pencil beamforming are necessary to ensure connectivity reliability in the above ~~100 GHz~~80 GHz regime, they may, at the same time, intensify the blockage challenges. Incorporating Reconfigurable Intelligent Surfaces (RIS) is a way to overcome blockage and reduce blocking probability.

## 7 Deployment scenarios and architectures

[840, 863] *[Editor's note: This section [840][is expected to describe] [863][addresses] typical use cases, deployment scenarios and network topologies for the deployment of IMT technologies in bands*

*above 100 GHz80 GHz. [877][Besides enhanced communication capabilities, new uses cases will be introduced such as integrated sensing and communication]]*

[877]

### 7.1 Use cases for IMT in bands above 100 GHz80 GHz

*[Editor's note: This section addresses typical use cases for IMT in bands above 100 GHz80 GHz.]*

Compared with the NR FR2 frequency band, the terahertz frequency band above 100 GHz80 GHz can provide a larger usable bandwidth, but it also suffers from greater path attenuation. Fortunately, it is possible to overcome certain path attenuation by improving the directivity and gain of the antenna and using beamforming technology to increase the coverage of the cell. IMT technologies adopted for bands above 100 GHz80 GHz can be used in indoor/outdoor hotspot environments, integrated sensing and communication and ultra-short-range environments to provide ultra-high data rate services. Some typical possible use cases are as follows.

**Indoor hotspot in a large meeting room**

The deployment adopts bands above 100 GHz80 GHz small cell base stations, which can solve the needs of applications with extremely high data rates, such as Holographic display etc. Environments such as large meeting room, have relatively closed environments. Outdoor macro and/or micro base station coverage are difficult to provide users with a sufficiently high data rate. Considering the large path attenuation of bands above 100 GHz80 GHz, high-gain directional antennas or large-scale antenna arrays that can provide higher gains can be used to flexibly establish wireless fronthaul /backhaul links with outdoor base stations or core networks. A single TRXP cannot support more users to use Holographic display application at the same time, so that a site may need to deploy multiple TRXPs. Deploying more dense base stations can provide better services to users, but it also brings interference problems. When using of bands above 100 GHz80 GHz, greater path attenuation and penetration loss may reduce the interference between adjacent cells.

**Integrated sensing and communication**

Integrated sensing and communication are an important technology trend in the future, which can save hardware resources to a considerable extent. A typical use case is the use of sensing technology to assist communication, such as using sensing technology to predict the user's trajectory to assist the base station in beam tracking of the user or using sensing technology to sense the user's location for rapid beamforming. Using bands above 100 GHz80 GHz can achieve better imaging and achieve higher positioning accuracy. [1062] Following use cases have been identified.

– High accuracy localization in an indoor factory/restaurant
– Simultaneous imaging, mapping and localization
– Augmented human sensing
– Gesture and activity recognition.

Below figure shows integrated communication and sensing/imaging in a radio access network (RAN). Either the base stations or the terminal devices can extract information about the object of interest in the surrounding environment from the received RF signals, such as existence, distance, speed, shape, and orientation. This information can be used for services such as localization and tracking, environment mapping and reconstruction as well as gesture/activity recognition, etc. Furthermore, it can also be used to improve the performance of communication services. With respect to the source of the RF signals, they may either be a communication signal or a dedicated

sensing signal. In terms of transmit and receive modes, the sensing may be performed by the device itself, or jointly performed by multiple devices.

FIGURE 6

**Integrated communication and sensing in a radio access network**
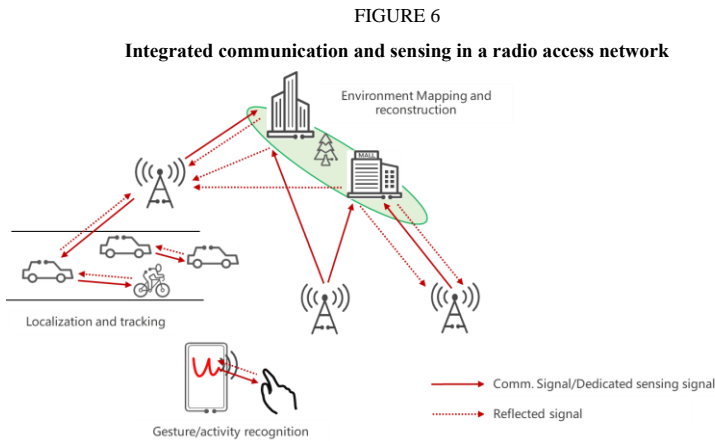


*Super-sidelink in short range communication environment*

Super-sidelink is a peer-to-peer communication link, which reuses the key features of the radio access links. It and the associated mesh networking is an integral part of the overall mobile network. Super-sidelink enables mobile devices to communicate with the nearby devices directly over short range distance. Therefore, the data traffic of the base station is offloaded, whereas the interaction delay between these mobile devices is also reduced. Device-to-device (D2D) and Vehicle-to-vehicle (V2V) communications are two representative super-sidelink communications. Below figure shows a use case of THz wireless super-sidelink communications.

FIGURE 7

**THz sidelink communications**
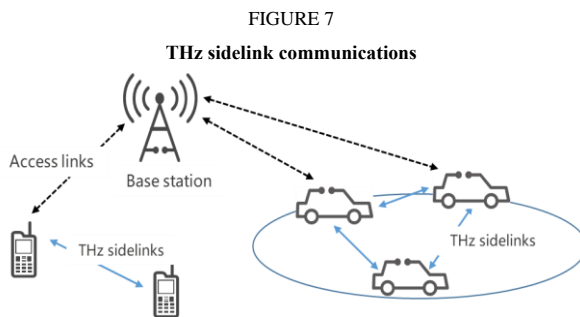


Recently, new wireless applications such as holographic interaction, automatic or assisted driving are emerged and have further requirements on bandwidth and transmission latency of communication links. It then is desirable to use super-sidelink communications in the THz frequency range.

*Flexible wireless backhaul*

With the increase of data traffic at the access point or base stations, new transmission capacity requirements are put forward for the backhaul of wireless networks. Terahertz provides a high-traffic transmission capability comparable to that of optical fibers. It is applicable to scenarios or environments where optical fibers cannot be deployed or are difficult to deploy, to satisfy the requirements for information exchange at extremely high data rates.

These access nodes may be in a form of a traditional base station, or may be a flexible deployed base stations with predictable deployment sites, such as a hovering aircraft or the infrastructure along a rail or road.

FIGURE 8

**THz flexible wireless backhaul**
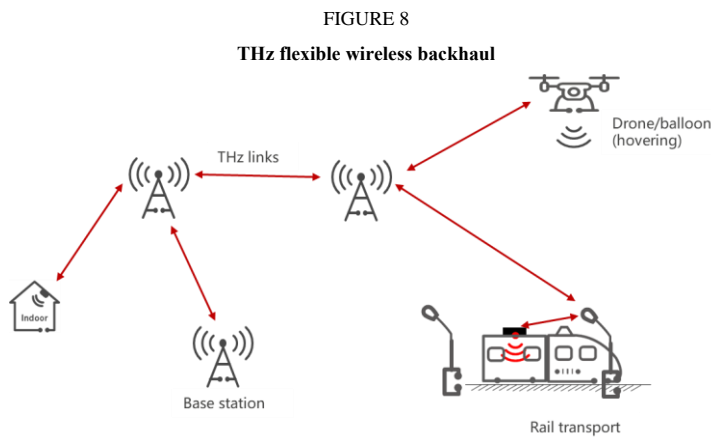


## 7.2 Deployment scenarios

*[Editor's note: This section addresses deployment scenarios for IMT in bands above ~~100 GHz~~80 GHz. Deployment scenarios include typical indoor/outdoor hotspot scenarios and some new scenarios, such as ultra-short-range scenarios for in-chip communication.]*

[975] Various deployment scenarios are envisaged for IMT in bands above 6 GHz. Deployment scenarios above ~~100 GHz~~80 GHz can include hot spot deployments, industrial networks, autonomous vehicles and smart railway networks [9]. It is challenging to use the tens of GHz bandwidth for a working system [2].

### 7.2.1 Hot Spot Deployments

Hot spot deployments are conventional applications, whereby extremely high data rate systems could be deployed indoors or outdoors. The low-frequency band above ~~100 GHz~~80 GHz (< 350 GHz) is well suited for such scenarios. Coverage radius in outdoor environments is limited to about 100 m because of high free space path loss and gaseous attenuation.

### 7.2.2 Industrial Networks

Industrial networks are envisaged to be privatized, focusing on extreme reliability and ultralow latency. Due to the strong beam directivity, high path loss, and large bandwidth of electromagnetic waves above ~~100 GHz~~80 GHz, it can provide higher reliability than the microwave.

### 7.2.3 Autonomous Vehicles and Smart Railway Networks

High-speed adaptive links between antennas on train rooftops and infrastructure can be used for the transmission of both safety-critical information and aggregate passenger data. High-frequency systems can also be used for access between UEs and antennas in the cabins that aggregate the passenger data, similar to a (moving) hotspot. These high-speed links are suitable for electromagnetic wave transmission above ~~100 GHz~~80 GHz.

### 7.3 Deployment architecture

*[Editor's note: This section addresses deployment architecture for IMT in bands above ~~100 GHz~~80 GHz. Compared with the architecture introduced in ITU-R M.2376, if there is a new deployment architecture, the differences need to be described.]*

### 7.3.1 Overlay network architecture

[1062] The overlay architecture refers to the network deployment of sub-THz wave small cells rolled out on of the existing macro networks. The existing macro cell layer is mainly used for coverage, and the micro cell layer adopted for bands above ~~100 GHz~~80 GHz is used for capacity boost.

An essential merit of such overlay network architecture is facilitating separation of control signalling and data transmission, where all control signalling is transmitted by existing macro cells and sub-THz small cells intend to provide high-rate data transmission only.

FIGURE

**Overlay network architecture**
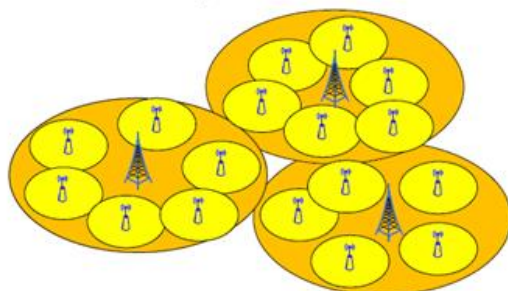


### 7.3.2 Wireless backhaul

[1062] In addition to the access network architecture, wireless backhaul is another key challenge for capacity requirements. As the average guaranteed network capacity increases and a large number of micro base stations are deployed, wired backhaul, such as optical fibers, is not feasible in many scenarios. Wireless backhaul is considered the optimal alternative.

In terms of the backhaul frequency, in-band backhauling or out-of-band backhauling are two alternatives. In-band backhauling has advantages in terms of spectrum efficiency and flexibility.

A combination of backhaul and access, i.e. integrated access and backhauling (IAB) is a promising deployment mode to solve large-capacity access and backhaul problems for IMT network in 2030 s.

FIGURE

**Wireless integrated access and backhauling architecture**
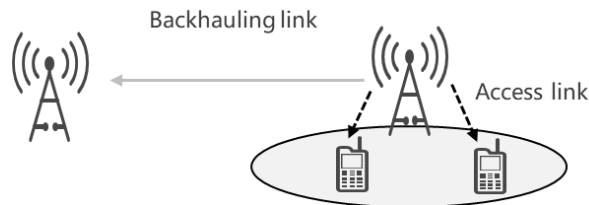


## 8 Conclusions

[863] *[Editor's note: To be described.]*

REFERENCES

*[Editor's note: To be added.]*

[1] Shafi M, Zhang J, Tataria H, et al., "Microwave vs. millimeter-wave propagation channels: Key differences and impact on 5G cellular systems," IEEE Communications Magazine, Vol 56, No. 12, December 2018.

[2] Tataria H, Shafi M, Dohler M, et al., "Six Critical Challenges for 6G Wireless Systems," arXiv preprint arXiv:2111.08871, 2021.

[3] Du K, Ozdemir O, Erden F, et al, "Sub-Terahertz and mmWave Penetration Loss Measurements for Indoor Environments," *2021 IEEE International Conference on Communications Workshops (ICC Workshops)*, June 14-23 2021.

[4] Kokkoniemi J, Petrov V, Moltchanov D, et al., "Wideband terahertz band reflection and diffuse scattering measurements for beyond 5G indoor wireless networks," *European Wireless 2016; 22nd European Wireless Conference*, May 18-20 2016.

[5] Akyildiz I F, Jornet J M, Han C., "Terahertz band: Next frontier for wireless communications," *Physical Communication*, Vol 12, pp. 16-32, September 2014.

[6] Hurley N, Rickard S., "Comparing measures of sparsity," *IEEE Transactions on Information Theory*, Vol 55, No. 10, October 2009.

[7] Zhang J, Tang P, Yu L, et al., "Channel measurements and models for 6G: current status and future outlook," *Frontiers of information technology & electronic engineering*, Vol 21, No. 1, March 2020.

[8] Priebe S, Kurner T., "Stochastic Modeling of THz Indoor Radio Channels," *IEEE Transactions on Wireless Communications*, Vol 12, No. 9, September 2013.

[9] Tataria H, Shafi M, Molisch A F, et al., "6G wireless systems: Vision, requirements, challenges, insights, and opportunities," *Proceedings of the IEEE*, Vol 109, No. 7, July 2021.

[1] H. Halbauer, T. Wild, "Towards Power Efficient 6G Sub-THz Transmission," Joint EuCNC & 6G Summit, June 8-11, 2021, Porto, Portugal

[2]     Hua Wang et. al., Fei Wang, Sensen Li, Tzu-Yuan Huang, Amr S. Ahmed, Naga Sasikanth Mannem, Jeongseok Lee, Edgar Garay, David Munzer, Christopher Snyder, Sanghoon Lee, Huy Thong Nguyen, and Michael Edward Duffy Smith, "Power Amplifiers Performance Survey 2000-Present," [Online]. Available: https://gems.ece.gatech.edu/PA_survey.html

[3]     M. Elkhouly et al., "D-band Phased-Array TX and RX Front Ends Utilizing Radio-on-Glass Technology," 2020 IEEE Radio Frequency Integrated Circuits Symposium (RFIC), 2020, pp. 91-94, doi: 10.1109/RFIC49505.2020.9218409.

[4]     S. Shahramian et. al., "A Fully Integrated 384-Element, 16-Tile, W-Band Phased Array with Self-Alignment and Self-Test", IEEE Journal of Solid-State Circuits, Vol. 54, No. 9, Sept. 2019

[5]     Nguyen Le Hang, Volker Braun, Hardy Halbauer and Thorsten Wild, "Waveform Comparison under Hardware Limitations for 6G Sub-THz Communications", in Proc. of IEEE Consumer Communications & Networking Conference (CCNC), 8-11 Jan. 2022

[6]     Hexa-X, "Deliverable D2.1: Towards Tbps Communications in 6G: Use Cases and Gap Analysis", Jun. 2021.

[7]     Hexa-X, "Deliverable D2.2: Initial radio models and analysis towards ultra-high data rate links in 6G", Dec. 2021.

[8]     M. Bozanic and S. Sinha, "Emerging Transistor Technologies Capable of Terahertz Amplification: A Way to Re-Engineer Terahertz Radar Sensors", Sensors 19 (11):2454, May 2019.

[9]     Franz Dielacher, et al, "SiGe BiCMOS Technology and Circuits for Active Safety Systems", International Symposium on VLSI Design, Automation and Test, Hsinchu, Taiwan, China, April 28-30 2014.

## Acronyms and abbreviations

*[Editor's note: To be added.]*

*[Editor's note: Annex(es) could be added for further detailed explanation for certain items above in sections as well as relevant test results, if needed.]*

## [841] ANNEX 1

Figure 1 shows the published measurement campaigns performed worldwide. The measurements have been conducted in both outdoor and indoor environments. There is a cluster of measurements done around the 140 GHz range and additional set of measurements performed above 260 GHz. For indoor campaigns in the 140 GHz range, we have results from New York University (NYU) Wireless **Error! Reference source not found.**, The French Alternative Energies and Atomic Energy Commission (CEA) Grenoble **Error! Reference source not found.Error! Reference source not found.**, Aalto University**Error! Reference source not found.** and Georgia Institute of Technology **Error! Reference source not found.**. Similarly for outdoor at 140 GHz, we also have results from University of Southern California **Error! Reference source not found.** and NYU Wireless **Error! Reference source not found.Error! Reference source not found.**. There is another cluster of measurements conducted above 260 GHz, all indoor, from Technische Universitat Braunschweig **Error! Reference source not found.**, Koc University **Error! Reference source not found.** and Georgia Institute of Technology **Error! Reference source not found.**.

FIGURE 1

**Summary of measurement campaigns above ~~100 GHz~~80 GHz**
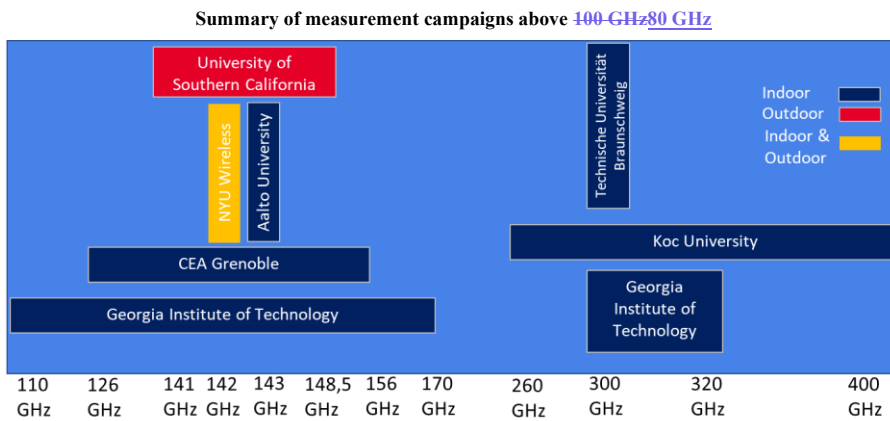


It would be useful to sub-divide the band into ranges as the interaction with materials in the environment will vary from 100-300 MHz Specifically, the lower edge of the band closer to ~~100 GHz~~80 GHz might expect performance similar to the channels already characterized by standards bodies such as the 3GPP, for example 100 to 115 GHz. A great deal of attention in measurement campaigns has been focused on the mid-range from 120 to 160 GHz with a particular focus on 140 GHz. Thus, characterizing in that range should be a priority. Lastly there have been several indoor studies in the higher frequencies at 300 GHz or range from 260 GHz to 320 GHz. 300 GHz can also be considered a separate range.

ANNEX 2

**Pathloss study on frequency band 140 GHz and 220 GHz in indoor scenarios**

## 1 Introduction

New spectral bands are required to support Terabit-per-second (Tbps) data rates for future wireless applications to deal with the exponential growth of wireless data traffic. To further move up the carrier frequency of millimeter-wave (mmWave) spectrum adopted already for IMT-2020, the Terahertz band spanning over 0.1 and 1 THz or even higher is envisioned as one of the promising spectrum bands to enable ultra-broadband 6G communications [1].

The channel measurement is the fundamental of the channel studies at bands above ~~100 GHz~~80 GHz. In this contribution, channel measurement campaign at 140 GHz and 220 GHz conducted in indoor meeting room and office environment will be introduced.

## 2 Channel measurement campaign

### A Channel sounder configuration

The channel measurement channel sounder consists of radio frequency (RF) fronts with horn antennas at bothTx and Rx sides, and a VNA. In 140 GHz measurement campaigns, the measured bandwidth $Bw$ is 13 GHz. Therefore, the delay domain resolution of our measurement results, $\Delta t = 1/Bw$, is 76.9 ps, which suggests two paths with the difference in propagation distance larger than 2.3 cm are resolvable. In addition, the number of the sampled points in the frequency domain or equivalently, the sweeping frequency points are 1301, which corresponds to the frequency interval of $\Delta f = 10$ MHz. The maximum detectable delay, $\tau_m = 1/\Delta f$, is calculated as 100 ns, hence, the largest traveling distance of a detectable path is $L_m = 30$ m. The details of the channel sounder configuration at 140 GHz and 220 GHz are summarized in Table 1.

TABLE 1

**Parameters of the measurement system**

| Parameter value | Value | |
|---|---|---|
| Sounder frequency | 140 GHz | 220 GHz |
| Local oscillator | 10.667 GHz | 18 GHz |
| Start frequency | 130 GHz | 221 GHz |
| End frequency | 143 GHz | 224 GHz |
| Bandwidth | 13 GHz | 3 GHz |
| Sweeping frequency interval | 10 MHz | |
| Sweeping points | 1301 | 301 |
| HPBW at Tx | 30º | 60º |
| HPBW at Rx | 10º | 10º |
| Delay resolution | 76.9 ps | 333.3 ps |
| Maximum excess delay | 100 ns | 1000 ns |
| Maximum path length | 30 m | 300 m |
| Azimuth rotation range | [0º, 350º] | |
| Elevation rotation range | [-20º, 20º] | |
| Rotation step | 10º | |

**B        Environment and measurement deployment**

The channel measurement campaigns were carried out in a typical meeting room and a typical office room. The meeting room is with an area of 10.15 m × 7.9 m and a ceiling height of 4 m as shown in Figure 1(a). And the dimension of the open office in our channel measurement campaign is 30m × 20m as shown in Figure 1(b). For meeting room, 12 positions of Rx are set in the meeting room. Tx A is close to a corner while Tx B is in the front of a wall of the meeting room. For office room, the measurement campaign consists of two sets, (i) open office area, (ii) office hallway. In the measurement set of open office area, Tx is placed at Tx B and Tx C, respectively. the distance between Tx and Rx varies from 3.5 m to 14 m. In the measurement set of office hallway, Tx is placed at Tx A while Rx is placed at A1-A21. The distance between Tx and Rx ranges from 2 m to 30 m.

FIGURE 1

**The deployment of the channel measurement in a (a) meeting room (c) office room.**



(a) Meeting Room          (c) Channel Sounder

(b) Office Room
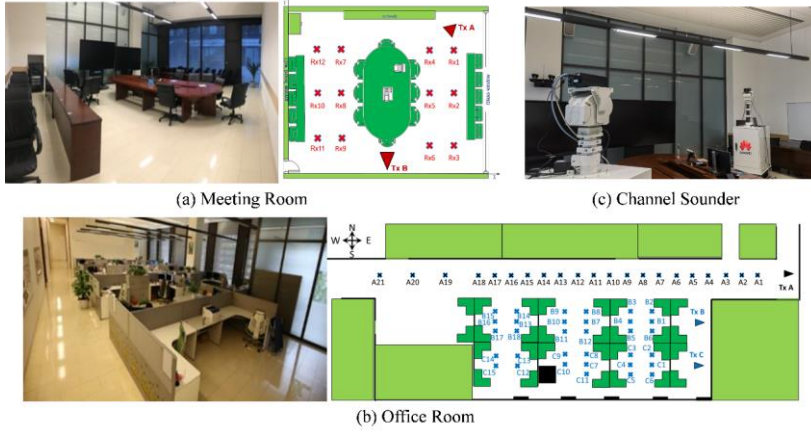
**3        Pathloss model**

Based on the measurement results, pathloss model for frequency band 140 GHz and 220 GHz bands is derived. ABG (alpha-beta-gamma) model is selected, which was introduced in [2]. And the ABG model was selected a mandatory model for IMT-2020 candidate technologies evaluation in 3GPP and ITU-R WP 5D [3][4]. The model is given as:

$$PL(f,d)[dB] = 10\alpha \log_{10}(d) + \beta + 10\gamma \log_{10}(f) + X_\sigma$$

where $\alpha$ captures how the pathloss increase as the transmit-receive in distance (in meters) increases, $\beta$ is a floating offset value in dB, $\gamma$ captures the pathloss variation over the frequency $f$ in GHz, and $X_\sigma$ is the shadowing fading term in dB.

The parameters for model in different deployment scenarios are summarized in Table 1.

TABLE 1

**Parameters for Pathloss model on 140 GHz and 220 GHz**

|  | $\alpha$ | $\beta$ | $\gamma$ | $\sigma$ [dB] |
|---|---|---|---|---|
| Meeting room | 2.33 | 17.66 | 2.56 | 2.68 |
| Open office area | 2.19 | 26.03 | 2.27 | 1.76 |
| Office hallway | 1.79 | 16.02 | 2.76 | 1.49 |

**Commented [Lin Hui10]:** Revisions proposed in 1062

It can be observed from Figure 2 to Figure 4, from the analysis of the path loss models, we observe that the dependence of path loss on distance, $\alpha$, in office hallway scenario shows the lowest $\alpha$ among all the scenarios due to the waveguide effect. While for the other two measured scenarios, the pathloss is close to the free space pathloss, which is give as:

$$\text{FSPL}(f,d) = 20\log_{10}(d) + 32.4 + 20\log_{10}(f)$$

FIGURE 2

**Path loss in the meeting room**
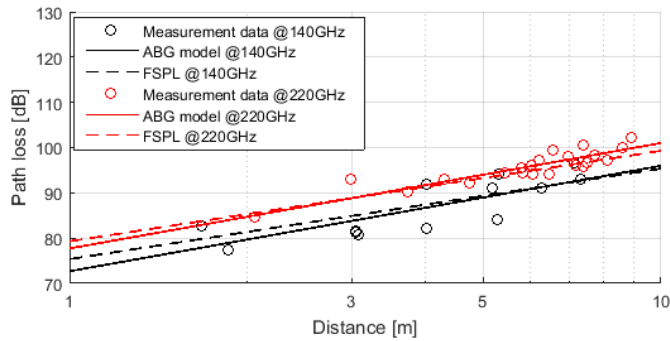


FIGURE 3

**Path loss in the open office area**
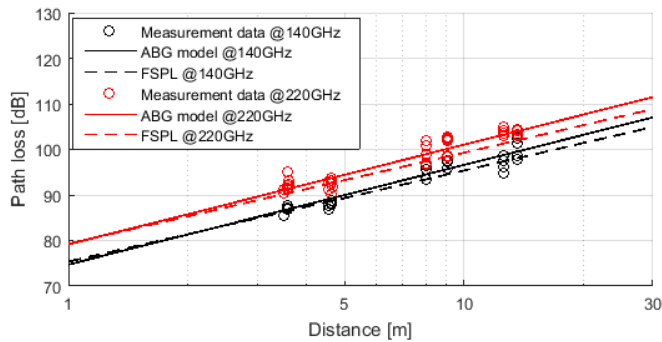
FIGURE 4

**Path loss in office hallway**
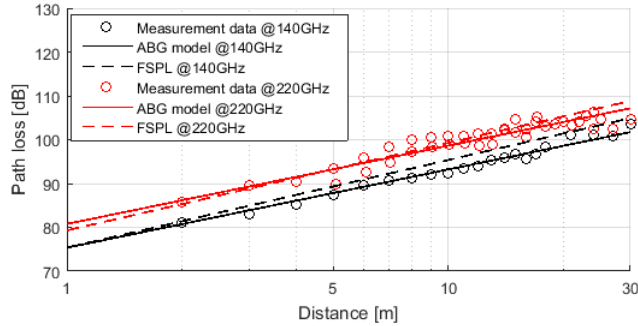


## 4 Conclusion

In this contribution, information about channel measurement campaigns conducted in indoor scenarios at 140 GHz and 220 GHz has been introduced. The measured indoor scenarios includes a meeting room, and office area, and hallway in office room. Pathloss models for the investigated bands are derived based on the channel measurement campaigns conducted in a meeting room and an office room. From the analysis of the path loss models, we observe that the dependence of path loss on distance, $\alpha$, in office hallway scenario shows the lowest $\alpha$ among all the scenarios due to the waveguide effect. And for the other two measured scenarios, the pathloss is close to the free space pathloss.

REFERENCES

[1]. W. Tong, P. Zhu, "6G: The Next Horizon, From Connected People and Things to Connected Intelligence", Cambridge University Press, 2021.

[2]. 5GCM, "5G channel model for bands up to ~~100 GHz~~80 GHz," Tech. Rep., Sep. 2016, Available online at http://www.5gworkshops.com/5GCM.html.

[3]. 3GPP TR 38.901, "Study on channel model for frequencies from 0.5 to ~~100 GHz~~80 GHz," v. 16.1.0, Dec. 2019.

[4]. ITU-R M.2412, "Guidelines for evaluation of radio interface technologies for IMT-2020," Sep. 2017.

[860] ANNEX 3

*Editor's note: More detailed information about spectrum analyzer settings, including RBW, VBW etc. are required.*

*Editor's note: Reply to the question above. The spectrum analyzer is working in IQ mode not in spectrum mode. The IQ signal is collected in time domain. So only "sampling rate" and "measurement samples" are needed to be set for the measurement. In order to avoid the misunderstanding, text is modified in the section 2-A.*

## Pathloss study on frequency band ranged from 220 GHz to 330 GHz in indoor short-distance scenario

## 1        Introduction

With the development of big data, the internet, cloud computing, smart city, and integration of multidimensional networks, the data traffic has grown continually [1]. To meet the future demand for mobile communication systems, higher frequency above ~~100 GHz~~80 GHz like Terahertz band (0.1-10 THz) has attracted considerable interests, which is considered as one of the promising spectrum bands for 6G.

Channel measurement is an effective and commonly used method of extracting channel properties. In this contribution, channel measurement campaign in the frequency range from 220 GHz to 330 GHz is conducted in the laboratory indoor short -distance scenario will be introduced.

## 2        Channel measurement campaign

### A        Channel sounder configuration

At the transmitter (TX) side, a vector signal generator (R&S SMW 200A) is used to generate the intermediate frequency (IF) signal. In the baseband, a periodic 12000 sample FrankZadoff-Chu (FZC) sequence with a duration of 5 µs was modulated using amplitude shift keying (ASK). For the frequency extender, it multiplies a local oscillator (LO) signal generated by a signal generator (R&S SMB 100A) with a factor of 18. Then, the IF signal is mixed with the LO signal and extended up into the THz range. A horn antenna with high gain is used to transmit the THz signal channel. At the receiver (RX) side, the transmitted signal is received by a horn antenna, and then is down-converted into the IF signal through a frequency extender. A spectrum analyzer (R&S FSW 43) which works in IQ mode, is utilized to demodulate the IF signal. In the baseband, 12000 IQ signal samples are recorded in time domain with a sample rate of 2.4 GHz. The antenna gain ranges from 24.8 dBi to 28.6 dBi. Half power beam width (HPBW) in the horizontal plane is about 7.5° while it is about 10° in the elevation plane. The details of the channel sounder configuration are summarized in Table 1.

TABLE 1

**parameters of the measurement system**

| Parameter value | Value |
|---|---|
| Sounder frequency | 220-330 GHz |
| Bandwidth | 2 GHz |
| Sample rate | 2.4 GHz |

| Parameter value | Value |
|---|---|
| Measurement samples | 12000 |
| Sequence duration | 5 µs |
| IF frequency | 2 GHz |
| LO frequency | 12.22-18.33 GHz |
| Antenna gain | 24.8-28.6 dBi |
| Antenna polarization | Vertical polarization |

## B        Environment and measurement deployment

A channel measurement campaign on a desktop as shown in Figure 1, was conducted in the frequency band of 220 GHz to 330 GHz. As shown in Figure 2, TX was fixed in the original point, and RX was moved along the line with a distance step of 0.1 m. A total of 20 LOS positions covering a distance from 0.1 m to 2 m were measured. In each measurement position, 22 frequency points have been measured including 12 frequency points from 220 GHz to 330 GHz with a step of 10 GHz and 10 frequency points from 234 GHz to 324 GHz with a step of 10 GHz.
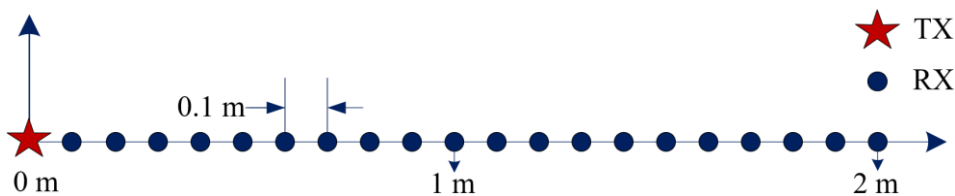
FIGURE 1

**The deployment of channel measurement**
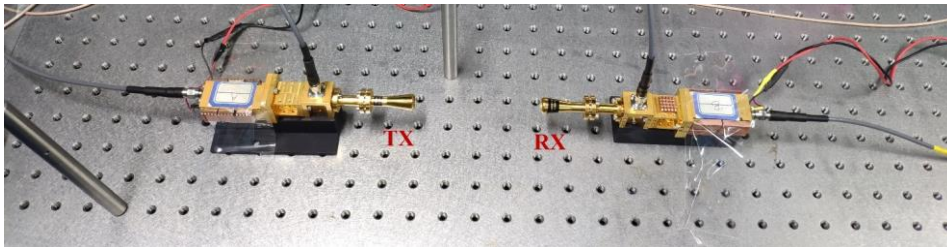


FIGURE 2

**The sketch map of measurement procedures**



## 3        Pathloss model

Three kinds of path loss models, i.e., the close-in (CI) model, the floating-intercept (FI) model, and the Alpha-Beta-Gamma (ABG) model, are always used to characterize the power attenuation during propagation [2], [3], [4]. The CI model and the FI model are both single-frequency path loss models. They can only model the path loss at one special frequency. The ABG model is a multiple-frequencies path loss model that can describe the fading in continuous bands. The CI model can be written as:

$$PL_{CI}(f,d)[dB] = PL_{FSPL}(f,d_0) + 10n\,log_{10}\left(\frac{d}{d_0}\right) + X_\sigma^{CI}$$

where $d_0$ is a physically-based reference distance, $n$ is the path loss exponent (PLE), and $X_\sigma^{CI}$ is a zero mean Gaussian random variable with a standard derivation of $\sigma$ in dB, which characterizes the shadow fading. $d_0$ is set to 0.1 m in this contribution. The CI model has only one variable $n$ that can be derived by using the minimum mean-square error (MMSE) approach, i.e., fitting the measured data with the smallest error. Thus, the complexity of the CI model is relatively low.

Compared with the CI model, the FI model does not consider the physical reference distance. It can be expressed as:

$$PL_{FI}(f,d)[dB] = \alpha + 10\beta\,log_{10}(d) + X_\sigma^{FI}$$

where $\alpha$ is the floating-intercept, $\beta$ is the slope of the model, and $X_\sigma^{FI}$ is a zero-mean Gaussian variable with a standard derivation $\sigma$ representing the shadowing. Similar to the CI model, two variables $\alpha$ and $\beta$ can be obtained by minimizing $\sigma$. Since the intercept is modeled as a variable, the FI model normally gets smaller $\sigma$ based on the same measured data compared with the CI model. This means that the FI model can predicate path loss more accurately in a specific environment. However, the CI model is more robust because it has a physical relationship to transmitted power.

We have conducted measurements at 22 frequency points from 220 GHz to 330 GHz. Due to the limit of space, we only plot the results at 230 GHz, 250 GHz, 270 GHz, 290 GHz, 310 GHz, and 330 GHz. But model parameters at all measured 22 frequency points are given in the following text. The parameters for models at twenty-two frequency points in scenario are summarized in Table 1. We can see that the CI model has a relatively larger standard derivation compared with the FI model. Furthermore, for the CI model, the frequency dependence of the PLE is not apparent. It gets the smallest PLE (1.83) at 310 GHz while it is 2.51 at 320 GHz. However, for the FI model, it seems that as the frequency increases, the slope has a decreasing trend. At 330 GHz, it gets the smallest slope (1.75).

TABLE 1

**Parameters for Pathloss models from 220 GHz to 330 GHz**

| Frequency (GHz) | CI model | | | FI model | | |
|---|---|---|---|---|---|---|
| | $PL_{FSPL}(d_0)$ $-10n\,log_{10}(d_0)$ /dB | $n$ | $X_\sigma^{CI}$ | $\alpha$ | $\beta$ | $X_\sigma^{FI}$ |
| 220 | 83.94 | 2.47 | 4.98 | 83.96 | 2.29 | 4.94 |
| 230 | 81.10 | 2.14 | 2.26 | 81.10 | 2.16 | 2.26 |
| 234 | 81.20 | 2.14 | 2.37 | 81.14 | 2.26 | 2.33 |
| 240 | 82.10 | 2.21 | 4.02 | 82.03 | 2.36 | 3.99 |
| 244 | 80.19 | 2.00 | 2.87 | 80.11 | 2.16 | 2.82 |
| 250 | 83.08 | 2.27 | 3.06 | 83.21 | 2.01 | 2.92 |
| 254 | 81.34 | 2.08 | 271. | 81.25 | 2.26 | 2.63 |
| 260 | 83.69 | 2.30 | 3.13 | 83.83 | 2.00 | 2.95 |
| 264 | 84.58 | 2.37 | 3.03 | 84.78 | 1.96 | 2.65 |
| 270 | 83.05 | 2.20 | 3.36 | 83.24 | 1.82 | 3.09 |
| 274 | 83.33 | 2.21 | 3.23 | 83.45 | 1.96 | 3.10 |

| Frequency (GHz) | CI model | | | FI model | | |
|---|---|---|---|---|---|---|
| | $PL_{FSPL}(d_0)$ $- 10n \, log_{10}(d_0)$ /dB | $n$ | $X_\sigma^{CI}$ | $\alpha$ | $\beta$ | $X_\sigma^{FI}$ |
| 280 | 84.60 | 2.32 | 4.15 | 84.85 | 1.80 | 3.71 |
| 284 | 82.36 | 2.09 | 3.33 | 82.50 | 1.79 | 3.17 |
| 290 | 85.10 | 2.34 | 3.71 | 85.35 | 1.83 | 3.25 |
| 294 | 86.75 | 2.49 | 3.65 | 86.99 | 1.98 | 3.17 |
| 300 | 85.21 | 2.32 | 4.05 | 85.49 | 1.75 | 3.50 |
| 304 | 85.48 | 2.34 | 4.13 | 85.68 | 1.93 | 3.86 |
| 310 | 80.52 | 1.83 | 2.78 | 80.56 | 1.75 | 2.77 |
| 314 | 81.90 | 1.95 | 3.02 | 81.86 | 2.03 | 3.00 |
| 320 | 87.59 | 2.51 | 4.18 | 87.93 | 1.80 | 3.36 |
| 324 | 85.34 | 2.27 | 3.35 | 85.59 | 1.75 | 2.80 |
| 330 | 84.81 | 2.20 | 3.42 | 85.02 | 1.75 | 3.02 |

Figure 3 shows measured path loss data, CI model results, and FI model results. The FSPL model and the ITU indoor hotspot path loss model are also plotted to do comparisons. The ITU indoor hotspot path loss model can be written as [4]:

$$PL_{ITU}(f,d)[dB] = 32.4 + 17.3 \, log_{10}(d) + 20 \, log_{10}(f).$$

This is a CI model with a PLE $n$ of 1.73. We can see that most circles are above the dotted line and the dash-dot line, representing the FSPL model and the ITU path loss model, respectively. This means that most measured path loss results are larger than the predication results of the FI model and the ITU model. And the actual propagation attenuation is severer. Though the measured distance is close, and it is like free space, the atmosphere absorption is not able to be ignored. The FSPL model and the ITU model both do not consider the atmosphere absorption. At some frequency points, e.g., 310 GHz, it is found that the propagation attenuation is not as severe as that in free space. This may result from physical reasons. For instance, with a special wavelength, the atmosphere absorption is relatively small. As discussed in, several spectrum windows with lower absorption losses exist. For the fitting results, it shows that the CI model and FI model both fit well with measured path loss samples. Also, these two models get similar fitting results. For example, at 270 GHz, the CI model line seems to overlap with the FI model line. These two models both perform well in predicting the path loss. Furthermore, there is a discrepancy between the fitting results and the ITU model. At 290 GHz, the discrepancy is about 4 dB between the FI mode line and the ITU model line.
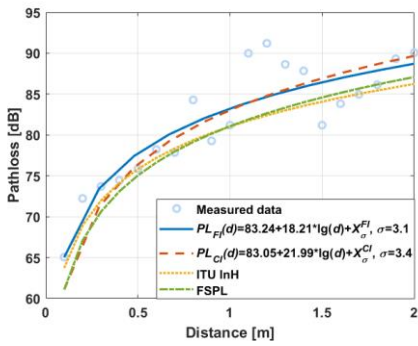
FIGURE 3

**Path loss results at 6 frequency points. The circles denote the averaged path loss samples at one distance. The solid line, dashed line, dotted line, and dash-dot line represents the FI model, the CI model, the ITU indoor hotspot model, and the FSPL model, respectively**
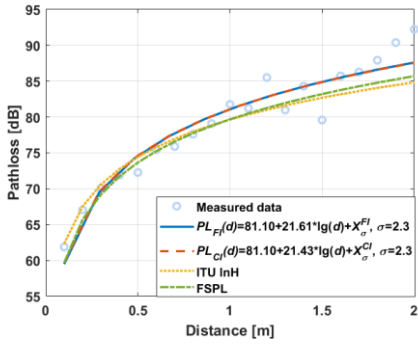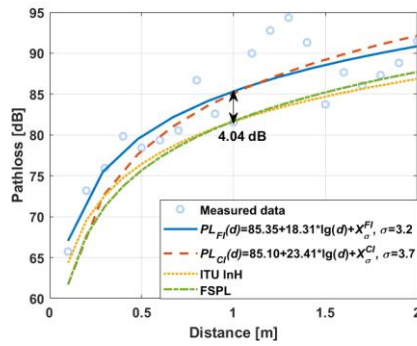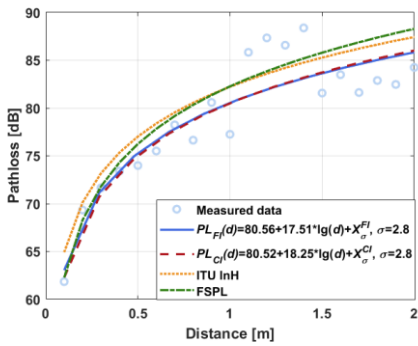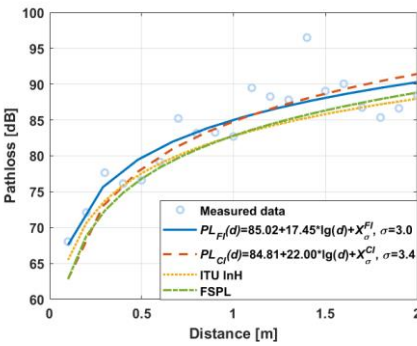


(a) 230 GHz
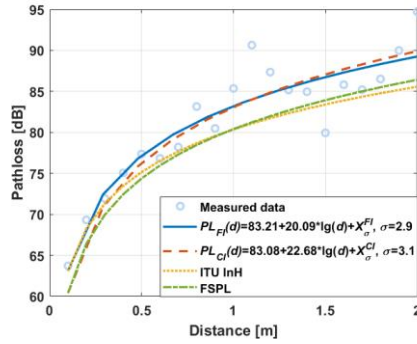
(b) 250 GHz

(c) 270 GHz

(d) 290 GHz

(e) 310 GHz

(f) 330 GHz

Frequency dependence plays an important role in understanding the channel characteristics in an extra-wide frequency range. To further investigate the frequency dependence of path loss, we use the ABG model to fit the measured path loss. The model is given as:

$$PL_{ABG}(f,d)[dB] = 10\alpha \, log_{10}\left(\frac{d}{d_0}\right) + \beta + 10\gamma \, log_{10}\left(\frac{f}{1 \text{ GHz}}\right) + X_\sigma^{ABG}$$

where $d_0$ is the received-power reference point (It is set to 0.1 m in this contribution), $\alpha$ and $\gamma$ are the distance and frequency dependence on path loss, respectively, $\beta$ is the optimized offset in path loss, and $X_\sigma^{AGB}$ has the same physical meaning with $X_\sigma^{FI}$. In this ABG model, we can see that path loss varies with the frequency and the spatial distance.

As shown in Fig. 4, the measured path loss and the ABG model are plotted. The derived parameters of the ABG model are $\alpha = 1.93$, $\beta = 13.27$, $\gamma = 2.1$, and $\sigma = 3.78$. It denotes that the frequency dependence is a little stronger than that in the free space.

FIGURE 4

**Multiple-frequencies path loss modelling results**
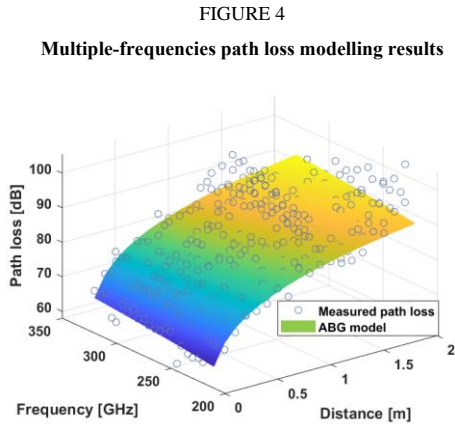


## 4 Conclusion

This contribution focuses on the path loss modelling and analysis in THz bands. Based on an extensive measurement campaign in the frequency range 220-330 GHz in an indoor shortrange scenario, we derive the path loss modelling results in 22 measured frequency points using the single-frequency path loss model. Also, the frequency dependence of path loss is investigated by fitting all measured data with a multiple frequencies path loss model. The obtained frequency exponent is 2.1. This indicates that there is a little stronger frequency dependence than that in free space. Furthermore, path loss variation over the measured bands is observed, which may be caused by atmosphere absorption.

REFERENCES

[1]. J. Zhang, P. Tang, L. Yu, T. Jiang, and L. Tian, "Channel measurements and models for 6G: Current status and future outlook," Frontiers of Information Technology & Electronic Engineering, vol. 21, no. 1, pp. 39–61, 2020.

[2]. 5GCM, "5G channel model for bands up to ~~100 GHz~~80 GHz," Tech. Rep., Sep. 2016, Available online at http://www.5gworkshops.com/5GCM.html.

[3]. 3GPP TR 38.901, "Study on channel model for frequencies from 0.5 to ~~100 GHz~~80 GHz," v. 16.1.0, Dec. 2019.

[4]. ITU-R M.2412, "Guidelines for evaluation of radio interface technologies for IMT-2020," Sep. 2017.

*Editor's note: This annex is incorporated from Document 5D/929-E from Samsung Electronics Co. Ltd*

# 1 Introduction

As new applications, such as virtual reality, create demand for ultra-high data rates beyond the capabilities of 5G-based mmWave systems [1]–[3], the wireless community naturally turns to higher frequencies, where the spectrum is less congested with existing services and larger bandwidths are available. In particular, the frequency range from 0.1-0.5 THz has been widely explored, e.g., [4]–[10] and is envisioned to be part of 6G wireless systems [11].

However, before any such systems can be designed and evaluated, an understanding of the unique propagation conditions in the THz band is required, since they can be significantly different from those at lower frequencies in the perspective of path loss, blockage, and reflection, etc.

In this contribution, we provide extensive channel measurement results for both LoS and NLoS (non-LoS) links in outdoor urban environments, including directional and omni-directional delay dispersion of the links [12][2].

# 2 Measurement equipment and site

## A Testbed description

Our channel sounder is based on a frequency-domain setup as shown in Figure 1. The basic principle of this channel sounder revolves around frequency extension of a vector network analyzer (VNA) signal into the THz domain by means of frequency multipliers. We introduce a RF-over-fiber (RFoF) link to allow the extension of the Rx beyond the distance limitations of a typical VNA-based THz channel sounding system (< 10 m). Due to the measurement principle of mechanically rotating antennas, every measurement lasted for several hours; measurements were done at night to ensure that no movement of people or vehicles was present in the environment.
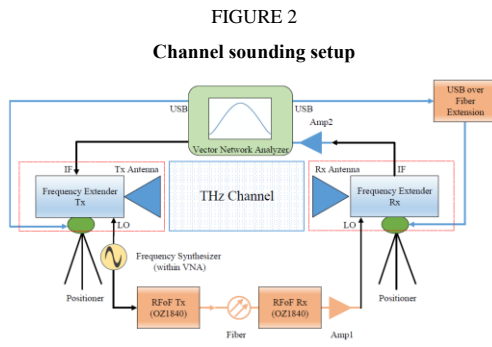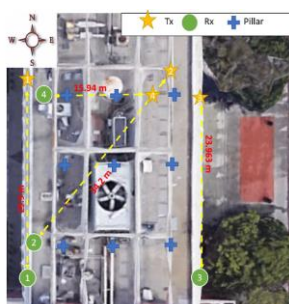
FIGURE 2

**Channel sounding setup**



_____

## B        Site description

For the measurements, we investigate an outdoor urban scenario. Specifically, our environment is located at the entrance of the Vivian Hall of Engineering (VHE) building in the USC University Park Campus, Los Angeles, CA, USA. It is an open space area with interspersed pillars (see Figure 2). On both sides of the entrance there are concrete walls and glass doors. The front side faces low height buildings and a street, and the back side faces an open area (quad) with several chairs, tables, trees, and a water fountain (this is the side shown in Figure 2(b)). For all our experiments the Tx and Rx were placed on paved ground.

FIGURE 3

**Measurement site**



(a) Measurement locations                                                    (b) VHE entrance view

The reported campaign consisted of 5 measurements in 4 different positions for Tx and Rx where each Tx location has its respective Rx location (Figure 2). For all Links, the height of the Tx and Rx was fixed to 1.65 m to emulate typical device-to-device (D2D) communication links. Link 1 (Tx1-Rx1) constitutes a LoS scenario case where Tx1 is in the northwest corner of the entrance and Rx1 is located at a distance of 29.9 m from it at the opposite side of the entrance. Link 2 (Tx2-Rx2) crosses the entrance diagonally; Tx2 is located at the northeast side of the entrance and Rx2 is located in the southwest corner. For this case, obstacles (i.e., pillars) are present on both sides of the LoS connection and the distance between Tx2 and Rx2 is 34.2 m. Similar to Link 1, Link 3 (Tx3-Rx3) is located on the opposite side of the entrance to where Link 1 is located, however, the length of this Link is 24.0 m. Note that Link 1 and Link 3 "see" different environments, as Link 3 has buildings on the east side, compared to Link 1 where we have an open area on the west side. Link 4 (Tx4-Rx4) is a NLoS link; for this case Tx and Rx have a geometrical distance of 15.9 m but 2 pillars block the LoS link between them. An additional measurement on Link 4 was performed to analyze the effect of increasing the reflectivity of the obstacles for the NLoS case. For this purpose, we wrapped all the pillars in the scenario with aluminium foil centered at 1.65 m as shown in Figure 3.

FIGURE 4

**Obstacles at VHE entrance**



(a) Without foil

(b) With foil
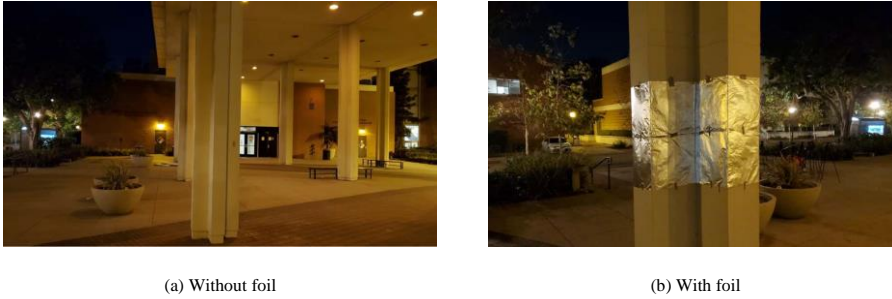
# 3 Measurement results

## A Measurement parameters

A summary of key measurement parameters, their acronyms and nominal values is given in Table I. The selection of 1 601 frequency points over 1 GHz of bandwidth provides a frequency resolution of 0.62 MHz which translates to 1.6 µs maximum excess delay or 480 m excess distance for multipaths to travel. In the current scenario, this is more than sufficient to capture all significant multipath components. The deployment of the positioners was done such that the angle of $0°$ for both the Tx and the Rx corresponds to the LoS for Link 1, 2 and 3. Tx and Rx face $90°$ away from each other in case of Link 4 measurements. The Tx scans a $90°$ ($-45°$ to $45°$) sector of the channel with a resolution of $5°$ in the azimuth. The Rx on the other hand looks at a full $360°$ with a $6°$ angular resolution. Since the antenna beam width is $14°$, any resolution below $7°$ is sufficient for comprehensive channel sounding.

TABLE 1

**Setup parameters**

| Parameter | Value |
| --- | --- |
| Measurement points | 1 601 |
| Start frequency | 145 GHz |
| Stop frequency | 146 GHz |
| Bandwidth | 1 GHz |
| IF bandwidth | 1 kHz |
| THz IF | 279 MHz |
| Antenna 3 dB beamwidth | $13°$ |
| Tx rotation range | $[0°,90°]$ |
| Tx rotation resolution | $5°$ |
| Rx rotation range | $[0°,360°]$ |
| Rx rotation resolution | $6°$ |

## B        LoS measurements

1)        Link 1: In Figure 4 (a), we first investigate the double-directional power angular spectrum, i.e., the power received for each combination of Tx and Rx direction, by employing a 30 dB threshold below the LoS, which is corresponding to the dynamic range of a typical communication receiver. Not surprisingly, most of the signal with high power is located around the LoS. Other regions of higher power are concentrated around the back of the Rx (−150° to 150°), which is due to strong reflections from the wall behind the Rx. Apart from these, we also see a smaller third cluster centered at almost 100° AoA and 10° AoD. This smaller cluster represents reflections off the pillar nearest to Rx as shown in the site map in Figure 2.

An omni-directional power delay profile (PDP), i.e., integrating the power delay profiles of the different horn orientations in Figure 4 (a) is shown in Figure 4 (b). We see that the biggest peak corresponds to the LoS link and the distance (converted from the measured delay by multiplying with the speed of light) for this peak corresponds to our measurements from the scenario. A number of other multipaths are also observed in channel that correspond to various reflective surfaces in the scenario with excess lengths of up to 150 m.
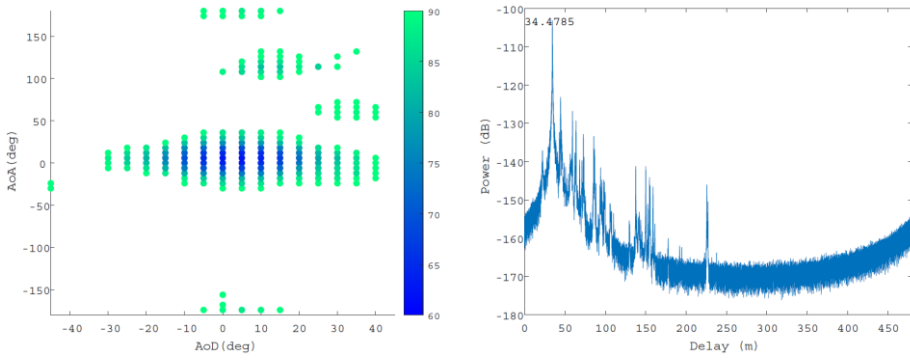
FIGURE 5

**Average pathloss per clusters and PDP for Link 1**



(a) Clusters within 30 dB of LoS                    (b) Omni-directional PDP for clusters within 30 dB of LoS
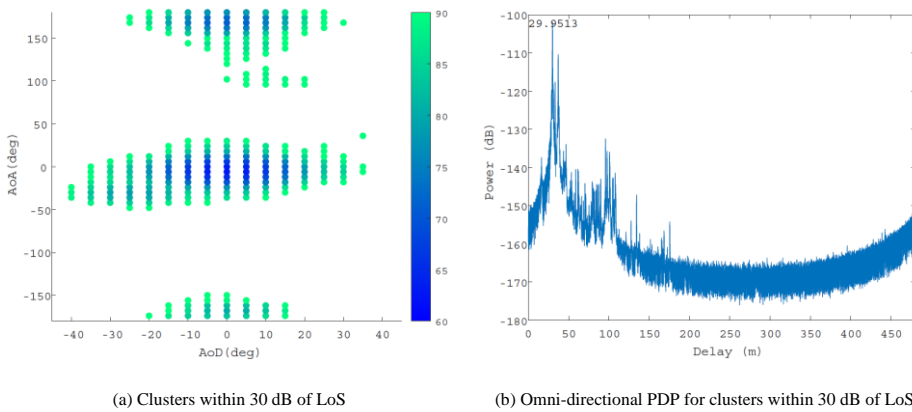
2)        Link 2: The major clusters for Link 2 are shown in Figure 5 (a). Although we do have a LoS cluster similar to Link 1, in this case we have only weak reflections from the back. The main reason for this is that instead of a wall on the back of Rx, in this case, we have some vegetation that does not have create strong specular reflections. Apart from this, we also see two other smaller clusters that correspond to reflections that go from the pillars to the buildings and finally end up at the Rx. The omni-directional PDP in Figure 5 (b) again shows the strongest peak from the LoS signal at a distance corresponding to the geometric distance, as shown in the scenario map in Figure 2. We see a higher number of multipaths, some of which have runlength greater than 200 m. This is because in this case we have a larger number of reflectors in the form of buildings and pillars available within the Tx's 90° sector.

FIGURE 5

**Average pathloss per clusters and PDP for Link 2**



(a) Clusters within 30 dB of LoS

(b) Omni-directional PDP for clusters within 30 dB of LoS

3)      Link 3: Figure 6 shows the clusters and omni-directional PDP for Link 3. The results are similar to those of Link 1 with strong LoS and a back-reflection clusters. The major difference is the absence of a pillar reflection similar to the one seen in Link 1. The reason for that is that propagation is along a road that has a thick cover of vegetation that blocks the connection from Tx to pillars. The PDP is similar to that of Link 1.

FIGURE 6

**Average pathloss per clusters and PDP for Link 3**
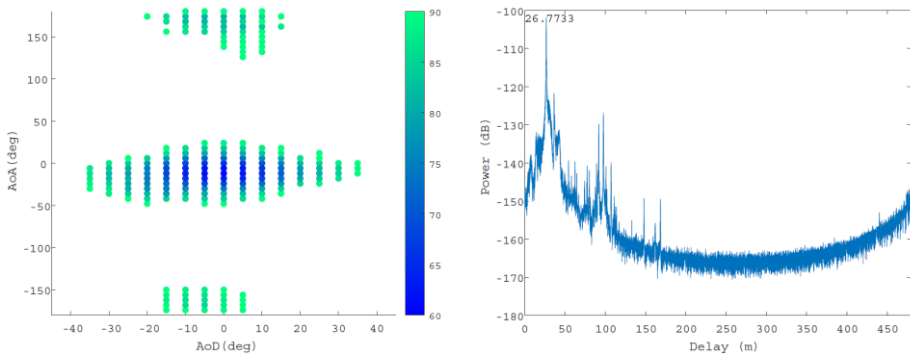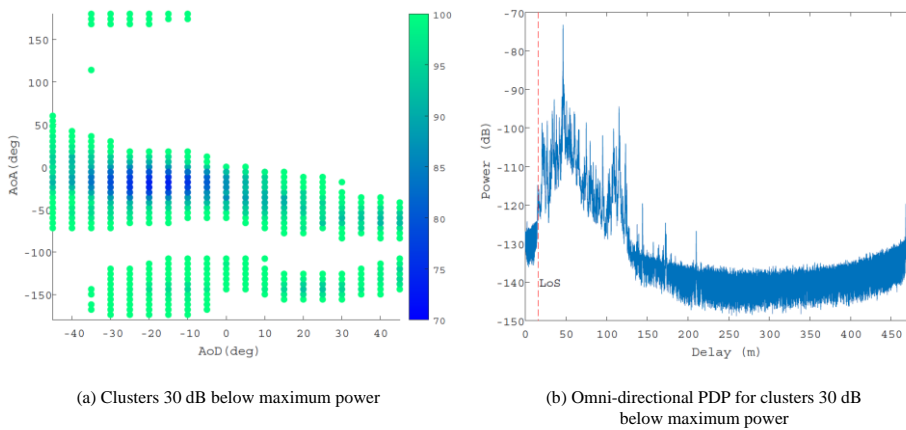


(a) Clusters within 30 dB of LoS

(b) Omni-directional PDP for clusters within 30 dB of LoS

## C        NLoS measurements

1)        Without reflective foil: The results for NLoS measurements of Link 4 without any reflective foil in the environment are shown in Figure 7. We see that even in this case several major clusters are present in the environment. From the 1140 direction pairs of Tx and Rx, we receive significant power in 411 pairs. These are all reaching the Rx through a number of paths in the channel. The PDP in Figure 7 (b) shows a very high multipath richness. The strongest path arrives after a detour of 46.35 m in the channel whereas there is no component at the LoS delay ($\approx$16 m) since a pillar blocks the LoS, and the Rx is not in the 90° sector that the Tx illuminates.

FIGURE 7

**Average pathloss per clusters and PDP for Link 4 without reflective foil**



(a) Clusters 30 dB below maximum power

(b) Omni-directional PDP for clusters 30 dB below maximum power

2)        With reflective foil: We now investigate whether multipath richness of the channel is further increased by the use of more reflective surfaces on various structures in the environment. As described in section 2, to achieve this, we use reflective foil on the pillars in the scenario. The increase in the number of significant (within 30 dB of the peak) direction pairs can be visually established by comparing Figure 7 (a) and Figure 8 (a). In all, 484 direction pairs have significant power, which is 73 more than the previous case. This shows that the use of reflective foil can significantly increase the multipath richness of the channel. The same can also be seen in the omnidirectional PDP where we not only have more multipaths but also their power is higher than the previous case.

- 46 -

FIGURE 8

**Average pathloss per clusters and PDP for Link 4 with reflective foil**



(a) Clusters 30 dB below maximum power

(b) Omni-directional PDP for clusters 30 dB below maximum power
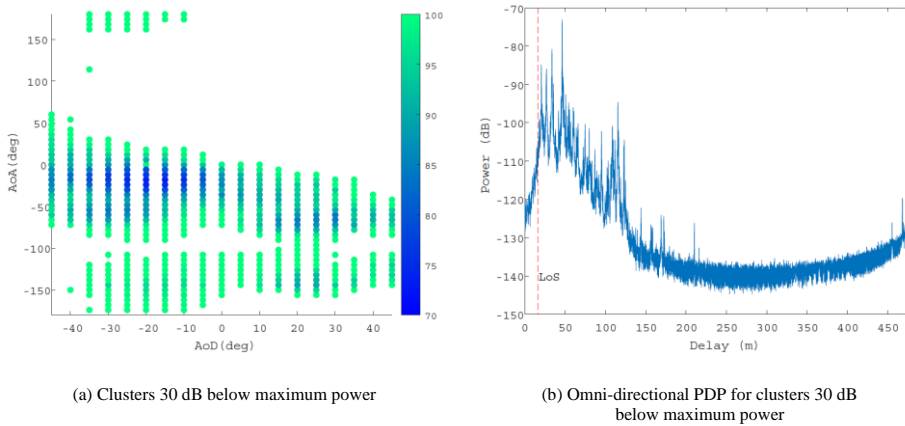
# 3    Conclusion

This contribution introduced measurement results of a double-directional (i.e., directional resolution at both link ends), ultra-wideband (1 GHz bandwidth) measurement campaign at 145 GHz carrier frequency. Measurements are done for D2D setups in an outdoor urban environment, with distances of 15-35 m between Tx and Rx.

The results showed a surprisingly rich multipath environment, leading to significant dispersion in both delay and angular domains. We also found that the specifics of the environment play a major role - concrete walls lead to much stronger reflections than vegetation, pillars and similar structures can be significant reflectors, and the building material impacts reflection coefficients and thus overall multipath richness, e.g., metallic coating (which is used, e.g., in energy-saving windows) reflects much more strongly than concrete surfaces.

REFERENCES

[1]    K.-C. Huang and Z. Wang, "Terahertz Terabit Wireless Communication," Microwave Magazine, IEEE, vol. 12, no. 4, pp. 108–116, June 2011.

[2]    V. Chandrasekhar, J. G. Andrews, and A. Gatherer, "Femtocell networks: a survey," IEEE Communications Magazine, vol. 46, no. 9, pp. 59–67, September 2008.

[3]    M. Shafi, A. F. Molisch, P. J. Smith, T. Haustein, P. Zhu, P. D. Silva, F. Tufvesson, A. Benjebbour, and G. Wunder, "5G: A Tutorial Overview of Standards, Trials, Challenges, Deployment and Practice," IEEE Journal on Selected Areas in Communications, 2017.

[4]    A. Hirata and M. Yaita, "Ultrafast Terahertz Wireless Communications Technologies," IEEE Transactions on Terahertz Science and Technology, vol. 5, no. 6, pp. 1128–1132, Nov 2015.

[5]    I. F. Akyildiz, J. M. Jornet, and C. Han, "TeraNets: ultra-broadband communication networks in the terahertz band," IEEE Wireless Communications, vol. 21, no. 4, pp. 130–135, August 2014.

[6]     H. J. Song and T. Nagatsuma, "Present and Future of Terahertz Communications," IEEE Transactions on Terahertz Science and Technology, vol. 1, no. 1, pp. 256–263, Sept 2011.

[7]     T. K¨urner and S. Priebe, "Towards THz Communications - Status in Research, Standardization and Regulation," Journal of Infrared, Millimeter, and Terahertz Waves, vol. 35, no. 1, pp. 53–62, 2014.

[8]     I. F. Akyildiz, J. M. Jornet, and C. Han, "Terahertz band: Next frontier for wireless communications ," Physical Communication, vol. 12, pp. 16 – 32, 2014.

[9]     N. A. Abbasi, A. Hariharan, A. M. Nair, and A. F. Molisch, "Channel measurements and path loss modeling for indoor thz communication," in 2020 14th European Conference on Antennas and Propagation (EuCAP). IEEE, 2020, pp. 1–5.

[10]    N. A. Abbasi, A. F. Molisch, and J. C. Zhang, "Measurement of directionally resolved radar cross section of human body for 140 and 220 GHz bands," in 2020 IEEE Wireless Communications and Networking Conference Workshops (WCNCW). IEEE, 2020, pp. 1–4.

[11]    H. Tataria, M. Shafi, A. F. Molisch, M. Dohler, H. Sj¨oland, and F. Tufvesson, "6G wireless systems: Vision, requirements, challenges, insights, and opportunities," 2020.

[12]    N. A. Abbasi, J. Gomez-Ponce, S. M. Shaikbepari, S. Rao, R. Kondaveti, S. Abu-Surra, G. Xu, C. Zhang, and A. F. Molisch, "Ultra-wideband double directional channel measurements for THz communications in urban environments," in ICC 2021-2021 IEEE International Conference on Communications (ICC). IEEE, 2021.

[1026] ANNEX 5

*Editor's note: This annex is incorporated from Document 5D/1026-E from Japan*

**Pathloss study on frequency band from 2 GHz to 300 GHz bands in urban microcell scenario**

## 1  Introduction

The initial pathloss measurement results from 2 GHz to 300 GHz conducted in urban microcell environment around the Tokyo station are introduced in this Annex.

## 2  Measurement Campaign

### 2.1  Measurement System Setup

The details of the measurement system setup at 2 GHz, 26 GHz and 300 GHz are summarized in Table 1. The Tx used these frequencies to transmit continuous wave (CW) signals, and the Rx measured path loss. The Tx antenna was set on the rooftop of a measurement vehicle with height of 2.8 m, which is lower than the surrounding building's rooftop level, as shown in Fig. 1(a). The Rx antenna was fixed to the trolley, with height of 1.7 m, as shown in Fig. 1(b). In 2 GHz and 26 GHz bands, the radiation patterns at the Tx and Rx antennas were omni-directional. On the other hand, the CW signal at 300 GHz was transmitted while the horn antenna with 10 degrees of half power beam width was rotated 360 degrees in the azimuth plane, and omni-directional antenna for Rx measured the CW signal.

TABLE 1

**Parameters of the measurement system**

| Parameter Value | Value | | |
|---|---|---|---|
| Frequency | 2 GHz | 26 GHz | 300 GHz |
| Signal | CW | CW | CW |
| Tx antenna | Omni-directional antenna | Omni-directional antenna | Horn antenna |
| Rx antenna | Omni-directional antenna | Omni-directional antenna | Omni-directional antenna |
| Half power beam width (HPBW) at Tx antenna | Approx. 360º in the azimuth plane Approx. 60º in the elevation plane | Approx. 360º in the azimuth plane Approx. 60º in the elevation plane | Approx. 10º in the azimuth plane Approx. 10º in the elevation plane |
| Half power beam width (HPBW) at Rx antenna | Approx. 360º in the azimuth plane Approx. 60º in the elevation plane | Approx. 360º in the azimuth plane Approx. 60º in the elevation plane | Approx. 360º in the azimuth plane Approx. 20º in the elevation plane |
| Tx antenna gain | 2.1 dBi | 2.0 dBi | 23.4 dBi |
| Rx antenna gain | 2.1 dBi | 2.0 dBi | 6.1 dBi |

FIGURE 1

**Tx and Rx antennas setup**
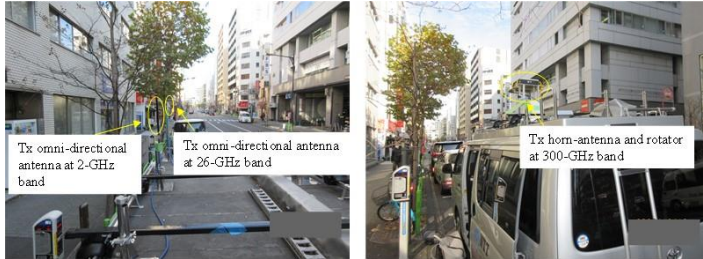


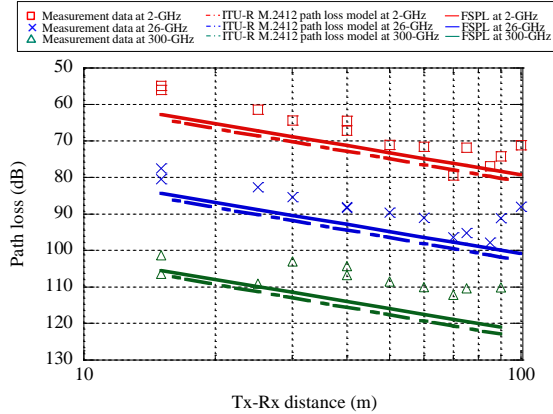(a) Tx antenna setup



(b) Rx antenna setup

## 2.2 Environment and Measurement Deployment

The path-loss measurement environment around Tokyo Station is shown in Figure 2. The typical urban microcell scenario is street canyon and the Tx is assumed to be well below the tops of surrounding buildings. The measurement environments around Tokyo station is therefore a typical urban microcell scenario as shown in Fig. 2. Path loss was measured at measurement points of the route 1, 2, and 3, as shown in Fig. 2(a). The distance from Tx to Rx is approximately from 8 to 90 m.
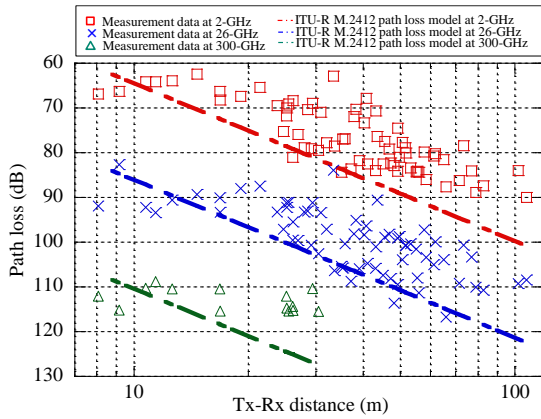
FIGURE 2

**The deployment of the pathloss measurement in an urban microcell environment**



(a) Measurement points          (b) Measurement environment

# 3    Measurement Results

We compared the free space path loss (FSPL), the Report ITU-R M.2412 pathloss model [1], and measurement results. The ITU-R M.2412 pathloss model was used a mandatory model for IMT-2020 candidate technologies evaluation in ITU-R. From Fig. 3(a), at the route 1, we observe that the measurement results shows the lower pathloss value than FSPL and ITU-R M.2412 pathloss model. The route mean square error (RMSE) between FSPL and measurement results is 5.26 dB at 2 GHz, 6.08 dB at 26 GHz, and 7.4 dB at 300 GHz. The RMSE between ITU-R M.2412 pathloss model and measurement results is 6.6 dB at 2 GHz, 7.56 dB at 26 GHz, and 8.8 dB at 300 GHz. It is assumed that the reflection and scattering from surrounding objects affects the pathloss characteristics in this street, therefore, the further analysis using the measurement data in various streets is needed. From Fig.3(b), at the route 2 and 3, the measurement data at the 2 GHz and 26 GHz bands show a similar tendency as the ITU-R M.2412 pathloss model. The RMSE between ITU-R M.2412 pathloss model and measurement results is 9.14 dB at 2 GHz, 8.67 dB at 26 GHz. On the other hand, measurement data at the 300 GHz band show a similar tendency as the ITU-R M.2412 pathloss model at the range from 8 m to 20 m of Tx-Rx distance, while we found that the measurement data at the 30 m is lower than ITU-R M.2412 pathloss model. The RMSE between ITU-R M.2412 pathloss model and measurement results is 8.9 dB at 300 GHz. Since the dynamic range is appox. 113 dB at the 300 GHz, measurement data could not be obtained.

FIGURE 3

**Measurement pathloss characteristics**



(a) Route 1



(b) Route 2 and 3

# 4      Summary

In this Annex, the information on initial pathloss measurement conducted in urban microcell scenarios from 2 GHz to 300 GHz has been introduced. Pathloss characteristics are investigated based on the measurement results. From the analysis results, we observe that the measurement pathloss in route 1 is lower than ITU-R M.2412 pathloss model due to the reflection and scattering from surrounding objects, and the measurement pathloss in route 2 and 3 show a similar tendency as the ITU-R M.2412 pathloss model at the 2GHz and 26 GHz. At the 300 GHz, measurement results show a similar tendency at the range from 8 m to 20 m of Tx-Rx distance, while we found that the measurement data at the 30 m is lower than ITU-R M.2412 pathloss model.

# REFERENCES

[1]     Report ITU-R M.2412, "Guidelines for evaluation of radio interface technologies for IMT-2020," Sep. 2017.

[1054] ANNEX 6

***Editor's note: This annex is incorporated from Document 5D/1054 from Rohde & Schwarz***

# 1    Introduction

This annex describes a channel measurement campaign performed in an urban micro and in an indoor scenario at 158 GHz and 300 GHz and presents first exemplarily results. The measurements are part of a larger research activity aiming for a better understanding of the millimeter and sub-millimeter (sub-THz and THz) mobile radio channel. The frequencies were chosen with respect to ongoing discussions for the sixth generation of mobile networks (6G). The presented results address fundamental questions with respect to the processing of measurement data and give some insight into typical properties of the radio channel at these frequencies.

# 2    Channel sounder

The measurements were captured using an instrument-based time-domain channel sounder. Figure 1 shows the setup used for 158 GHz and Figure 2 the setup for 300 GHz. Both comprise at the transmitter a broadband vector signal generator to generate an IF signal from a digital baseband sequence as well as a single-sideband upconverter with distinct LO source, bringing the signal into the RF domain. At the receiver side, the antenna signal is amplified and mixed into an IF domain by means of a downconverter and LO generator. The IF signal is sampled within a signal analyzer and the IQ samples are stored for further processing. Transmitter and receiver are synchronized with two Rubidium-based reference clocks and trigger units (Synchronomat) enabling coherent measurements and allowing for the evaluation of phase and coherent averaging as well as the determination of the absolute time-of-flight. Further information about the setup can be found in [1].

The receiving antenna could be rotated in the azimuth plane by means of a positioning unit to allow for stepwise angle resolved measurements. The receiver was mounted on a cart (camera dolly) for easily and precise movement to the different receiver positions.

The described setup has been already successfully used for measurements at 300 GHz as described in [2] and [3].
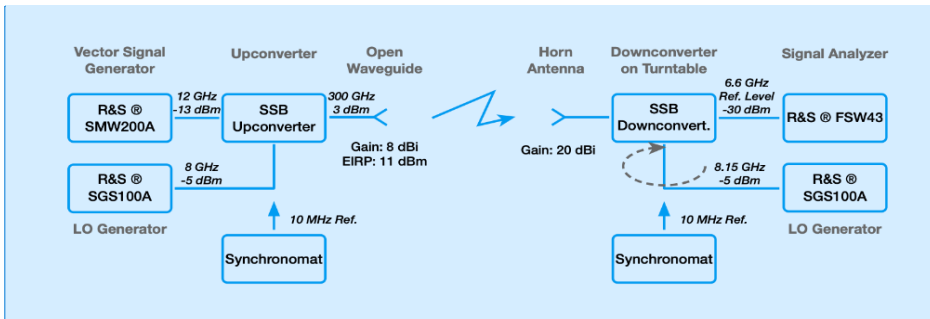
Table 1 summarizes the essential technical parameters of the time-domain channel sounder. Using a configuration with perfect complex correlation sequences (Frank-Zadoff-Chu sequences) and with additional coherent averaging after estimation and compensation of drift due to phase noise, enables a large processing gain and an exceptionally high dynamic range. Fundamental assessments of the utilized time-domain channel sounding principle can be found in [4].

FIGURE 1

**Measurement for 158 GHz**
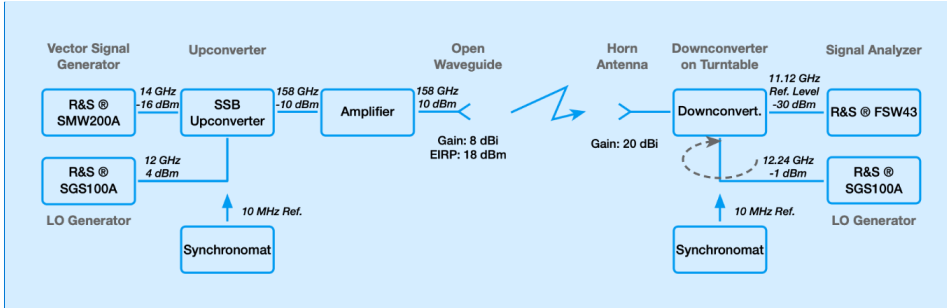
FIGURE 2

**Measurement setup for 300 GHz**

TABLE 1

**Measurement parameters for 158 GHz and 300 GHz**

| Paramater | Value @ 158 GHz | Value @ 300 GHz |
|---|---|---|
| Frequency | 158 GHz | 300 GHz |
| Bandwidth | 2 GHz | 2 GHz |
| Temporal resolution | 0.5 ns | 0.5 ns |
| Sequence | Frank Zadoff Chu | Frank Zadoff Chu |
| Period Length | 200,000 samples | 200,000 samples |
| Period Duration | 100 µs | 100 µs |
| Number of Measured Periods | 250 | 250 |
| Measurement Duration | 25 ms | 25 ms |
| Theoretical Processing Gain | 77 dB | 77 dB |
| Dynamic Range | > 70 dB | > 70 dB |
| Transmit Power | 10 dBm | 3 dBm |
| Tx Antenna Gain | 8 dBi | 8 dBi |

| Paramater | Value @ 158 GHz | Value @ 300 GHz |
|---|---|---|
| e.i.r.p. | 18 dBm | 11 dBm |
| Rx Antenna gain | 20 dBi | 20 dBi |
| Angular Resolution | 15 degree (24 steps) | 15 degree (24 steps) |

# 3        Measurement scenario

The measurements took place on company premises in Munich, Germany, well representing an urban micro street canyon scenario and an indoor shopping mall scenario. Figure 3 shows a map of the investigated scenario. The outdoor measurements were performed between the two grey marked buildings on the left side of the map. The width of the street is 15.5 m and each building has a height of approx. 20 m. The transmitter was located at the marked position at the left border of the map at a height of 1.5 m. The receiver was moved on multiple positions along the street and up to a maximum distance of 170 m. Most of the measurements were in a line-of-sight situation. The receiving antenna was mounted at a height of 1.5 m as well.

The indoor measurements were performed in a large open space in the building at the right side of the map, mimicking a shopping mall or airport scenario. The size of the hall is approx. 52 m x 13 m with a height of the ceiling of around 20 m. The transmitter was situated at the left side of the hall (antenna height 1.5 m) and the receiver (antenna height 1,5 m) was again moved to distinct positions on a rectangular grid. The maximum distance was 50 m and all positions were line-of-sight. Figure 4 shows two pictures of the investigated scenarios.

FIGURE 3

**Map of the investigated scenarios: street canyon (left), indoor shopping mall (right). The positions of the transmitter are marked with red stars, the positions of the receiver with green ones**
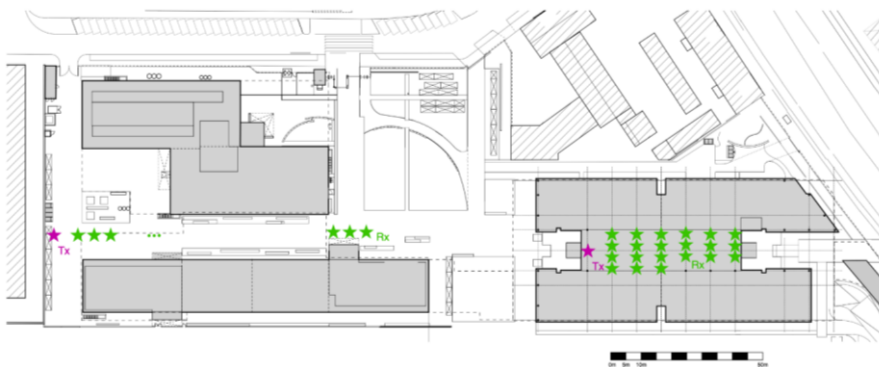
FIGURE 4

**Photograph of the street canyon, facing towards the right side of the map (left picture) and of the hall, facing towards the transmitter position (right picture)**



# 4          Discussion of first results

The received IQ samples were stored in the signal analyzer and were transferred as raw measurement data to a computer after completion of the measurements. The following postprocessing of the data includes resampling and filtering of the time domain samples, estimation of the common phase drift per sequence period and compensation of the phase drift, coherent averaging of all sequence periods, correlation and the application of amplitude and phase corrections by utilizing data from back-to-back calibration measurements. The results are absolutely calibrated channel impulse responses, sampled at Nyquist rate and with magnitudes corresponding to the gain of the communication channel (including the antennas) and delays corresponding to the tine of flight. These channel impulse responses (CIR) are generic, could be exchanged with other researches and are the basis for former evaluation.

**Aligned Measurement**

The most straight-forward evaluation of the CIRs is the application of a frequency domain window to suppress the side-lobes in the delay domain and to investigate the resulting (windowed) CIRs as instantaneous realizations of the radio channel. The Figure 5 shows the CIR for aligned antennas in the outdoor scenario at a distance of 30 m for both frequencies (after application of an ultraspherical window in with 80 dB suppression and parameter 1).

One recognizes the delay (time-of-flight) of 0.1 µs of the first peak, corresponding to a distance of 30 m. From the diagrams, the noise floor at 158 GHz can be estimated to around -140 dB, whereas the noise floor for 300 GHz is around -130 GHz. Both are exceptional high values for this frequency range. This difference corresponds to the unequal transmit powers (10 dBm versus 3 dBm) and the higher noise figure of the receiver at 300 GHz. The channel gains of the strongest path differ by 1-2 dB from the theoretically expected values (from free-space-loss and antenna gains) which is acceptable, since the depicted CIRs are not oversampled, i.e., the maximum might not be caught and the antenna gains at the transmitter side were not exactly known.

FIGURE 5

**Instantaneous CIR at 30 m distance for 158 GHz (left) and 300 GHz (right), with aligned antennas**
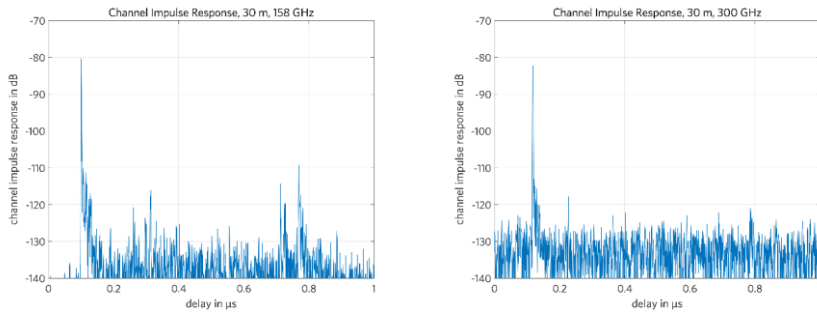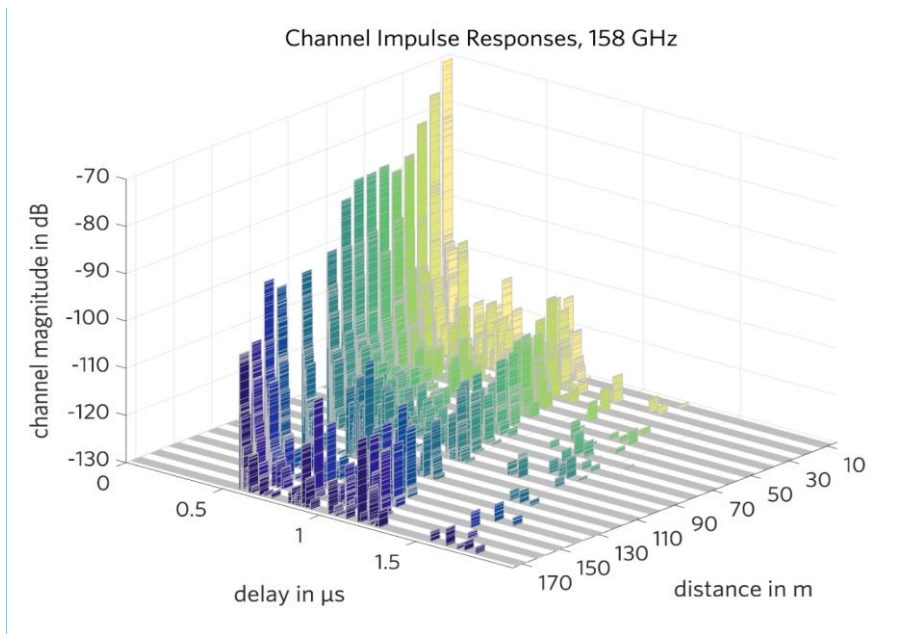
Figure 6 shows the instantaneous CIRs in the outdoor scenario over distance for 158 GHz. These measurements cover the complete length of the street between the two buildings. The antennas were always aligned. From this set of large-scale measurements, the path loss exponent can be resolved afterwards.

FIGURE 6

**CIRs at 158 GHz with aligned antennas over distance**

**Angle Resolved Measurements**

Further evaluations of the measured data sets comprise the investigation of the angular information. At each measurement point the receiver was rotated to 24 equal spaced angular positions, resulting in a spatial scanning of the radio channel in the azimuth plane with 15 degree resolution. One straight-forward way is, to study the overlay of all CIRs for all 24 angles of the received antenna, to get an insight into the spatial richness of the channel. Figure 7 shows such an overlay in form of the envelope of all CIRs gathered at 30 m (outdoor scenario) at 158 GHz. In comparison with Figure 5 (left plot), where the CIR for the main line-of- sight direction is drawn, one observes much more multipath components. For this envelope plot, the CIRs have been interpolated (oversampled) to enable a better resolution of the maximum values of the peaks.

FIGURE 7

**Envelope plot of all measured directions at 30 m distance (outdoor scenario)**



Power Envelope of all Angles, 30 m, 158 GHz
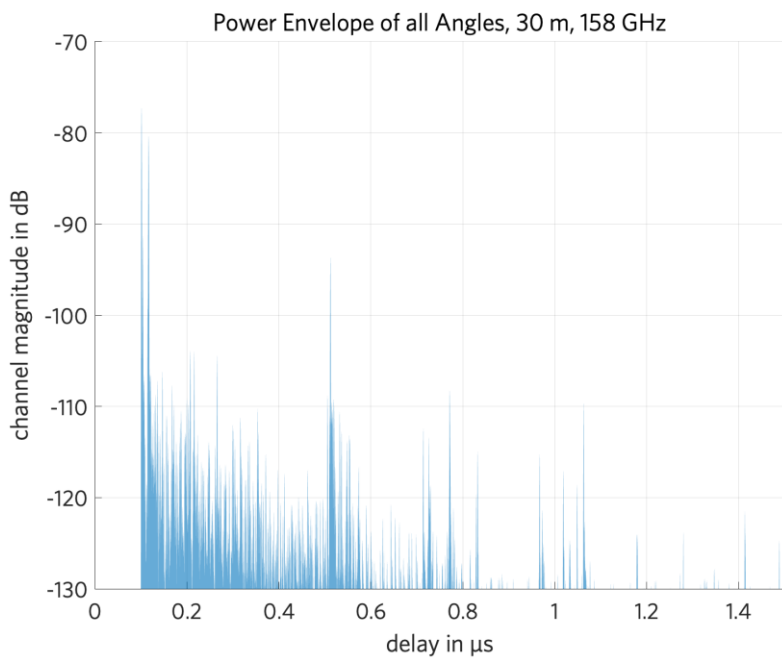
Commented [MC14]: Updated figured provided during offline email discussion by Taro Eichler of Rhode Schwarz

Figure 8 compares the envelope plots of 158 GHz (with zoomed delay axis compared to Figure 7) and 300 GHz at the 30 m position (outdoor), to get a direct insight into the frequency dependency. It could be clearly observed that the channel at 300 GHz is much sparser than the channel at 158 GHz, showing just two clusters of multipath components and having a much shorter channel length (maximum excess delay). This might be partly due to the higher noise floor at 300 GHz in combination with a 5.6 dB stronger decay at 300 GHz compared to 158 GHz, but this does not completely explain the observed result.

FIGURE 8

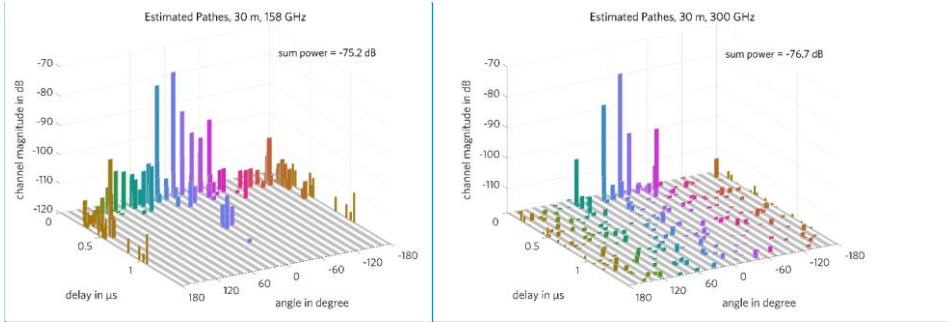**Power envelope at 158 GHz and 300 GHz for 30 m distance (outdoor)**
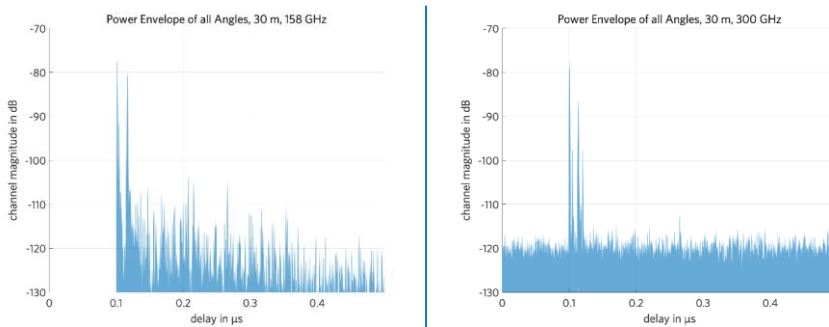


**Commented [M(15)]:** Updated figured provided during offline email discussion by Taro Eichler of Rhode Schwarz

Since the receiver antenna does not apply an ideal spatial filtering of 15 degree width, there is some leakage between adjacent angular measurements and further processing of the data is required to estimate individual paths and to calculate accurate sum powers. A feasible method is, to determine the local maxima of the CIRs evaluated in the (cyclic) angular delay domain [2], [3]. With that, the leakage of the main antenna beam to neighboring "angle bins" is suppressed, whereas sidelobes of the antenna patterns could still produce responses at other angles. Therefore, antennas with low sidelobe levels (Gaussian Beam antennas ideally) are preferable for this type of measurements. The Figure 9 shows the result of such a path estimation for both frequencies and the same measurement point (30 m, outdoor). It has to be noted, that the angle axis represents a cyclic dimension, which means that the first and the last row in these plots are identical, which is also reflected by the colors. For these evaluations a proper control of the noise threshold is necessary, to clearly discriminate the signal paths from noise. For the example given in Figure 9 the absolute noise thresholds were set to -130 dB for 158 GHz and to -118 dB for 300 GHz.

FIGURE 9

**Estimated paths in delay angle domain for 30 m distance (outdoor) and 158 GHz (left) and 300 GHz (right)**

With this estimation of paths, it is possible to sum up the overall received power (i.e., effective overall path gain) from all paths, as also indicated in the plots. Although the channel at 300 GHz is much sparser than the channel at 158 GHz one can clearly notice from the overall power, that there is no large difference in the overall power. Essentially one would expect that the overall power at 300 GHz is around 6 dB less, compared to 158 GHz, which is not the case. Such, it can be concluded, that the additional paths at 158 GHz could be resolved due to the high sensitivity of the measurement principle though, but do not significantly contribute to the overall power.

Moreover, statistical parameters like rms delay spread and rms angular spread can be evaluated from these results. In doing so, a fixed noise threshold is less useful than a relative noise threshold compared to the received power, to achievable comparable results.

Another interesting representation of the results could be done by means of rose plots as shown in Figure 10. Here each "pie" represents the overall power in the respective angle bin, normalized to the overall power. The single contributions from distinct paths within one angle bin are depicted by dots. Again, one can clearly see, that only one or two angle bins account for almost all the overall power and that within one bin only a few paths contribute significantly.

FIGURE 10

**Rose plot for 30 m distance (outdoor) and 158 GHz (left) and 300 GHz (right)**
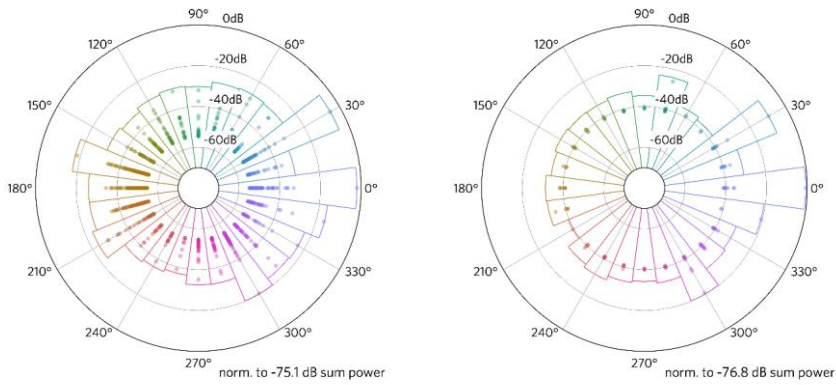


Finally, the Figure 11, shows an example of the indoor measurements at 158 GHz at a distance of 40 m. As expected, there are more multipath components from different directions contributing to a larger overall received power, compared to the outdoor measurements (-71.4 dB at 40 m vs. -75.1 dB at 30 m).

FIGURE 11

**Estimated Paths of one indoor position at 158 GHz**
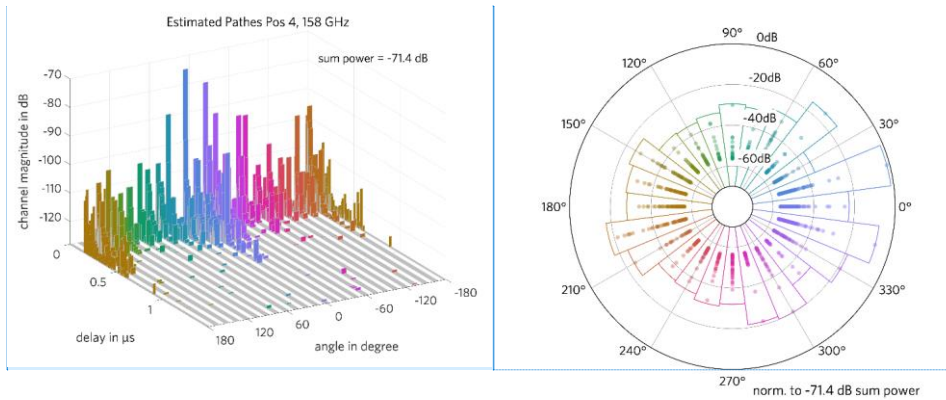


> **Commented [MC17]:** Updated figured provided during offline email discussion by Taro Eichler of Rhode Schwarz

## REFERENCES

[1]    M. Schmieder et al., "THz Channel Sounding: Design and Validation of a High
        Performance Channel Sounder at 300 GHz," 2020 IEEE Wireless Communications and
        Networking Conference Workshops (WCNCW), 2020, pp. 1-6,
        doi: 10.1109/WCNCW48565.2020.9124887.

[2]    F. Undi, A. Schultze, W. Keusgen, M. Peter and T. Eichler, "Angle-Resolved THz
        Channel Measurements at 300 GHz in an Outdoor Environment," 2021 IEEE
        International Conference on Communications Workshops (ICC Workshops), 2021,
        pp. 1-7, doi: 10.1109/ICCWorkshops50388.2021.9473891.

[3]    A. Schultze, ] F. Undi, M. Peter, W. Keusgen and T. Eichler , "Angle-Resolved THz
        Channel Measurements at 300 GHz in a Conference Room Environment,"URSI GASS
        2021, Rome, Italy, 28 August - 4 September 2021.

[4]    S. Wittig, W. Keusgen, M. Peter and T. Eichler, "On the Dynamic Range of Digital
        Correlative Time Domain Radio Channel Measurements, " arXiv:2008.07805.

[1062] ANNEX 7

*Editor's note: This annex is incorporated from Document 5D/1062-E from China (People's Republic of)*

## Study on the dependence of rain attenuation on the rain drop dimension

[1] presents results from research activity on EM wave propagation conducted in Milan, which has installed and operated since 2016 two parallel full-duplex terrestrial radio links connecting two buildings in the Politecnico di Milano main campus. The links work in the E (73 and 83 GHz) and D (148 and 156 GHz) bands and are 325-m long. A disdrometer located at one hop position allows to measure rain drop distribution and to evaluate rain attenuation. The key role of the rain microphysics can be seen in the following pictures, displaying one rain event with rain rate (Fig. 1) and rain attenuation (Fig. 2) on the D band link according to ITU-R model P.838-3 and according to the estimation based on DSD data, both compared to the measured attenuation:
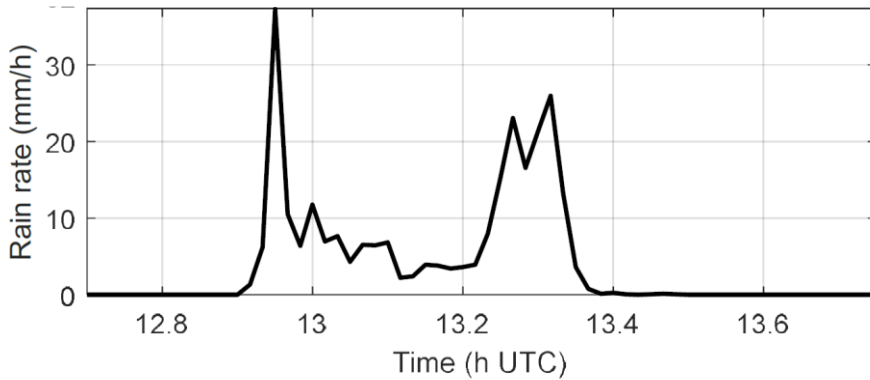
FIGURE 1

**Sample identification of a rain event**



FIGURE 2

**Rain attenuation estimated by Recommendation ITU-R P.838-3, estimated by DSD data and measured**
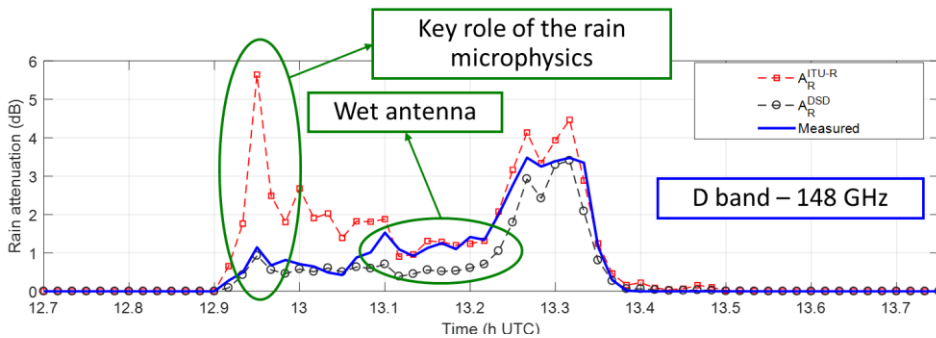
Figure 2 shows that the estimation of rain attenuation based on DSD data is much more accurate than the estimation based on Recommendation ITU-R P.838-3.

The so called "wet antenna" effect is investigated as well, due to the thin wet film which is generated by rain on the surface of the antenna provoking some additional attenuation.

It's also worthwhile to note that the same situation in which the DSD based evaluation is more accurate than the Recommendation ITU-R P.838 based evaluation is found on the E band link, showing that the impact of rain microphysics on the path attenuation is already relevant at E band, where the wavelength begins to be comparable to the rain drop size.

Further activity is ongoing in order to identify possible models that could enhance Recommendation ITU-R P.838 in the evaluation of the impact of rain on radio propagation at frequencies over ~~100 GHz~~80 GHz.

## REFERENCES

[1]      L. Luini, G. Roveda, M. Zaffaroni, M. Costa and C. Riva, "EM wave propagation experiment at E band and D band for 5G wireless systems: Preliminary results," 12th European Conference on Antennas and Propagation (EuCAP 2018), 2018, pp. 1-5, doi: 10.1049/cp.2018.0378.